

Enhancing Neural Adaptive Wireless Video Streaming via Lower-Layer Information Exposure and Online Tuning (Technical Report)

Lingzhi Zhao, Ying Cui, *Member, IEEE*, Yuhang Jia, Yunfei Zhang, Klara Nahrstedt, *Fellow, IEEE, ACM*

Abstract—Deep reinforcement learning (DRL) demonstrates its promising potential in the realm of adaptive video streaming and has recently received increasing attention. However, existing DRL-based methods for adaptive video streaming use only application (APP) layer information, adopt heuristic training methods, and train generalized neural networks with pre-collected data. This paper aims to boost the quality of experience (QoE) of adaptive wireless video streaming by using lower-layer information, deriving a rigorous training method, and adopting online tuning with real-time data. First, we formulate a more comprehensive and accurate adaptive wireless video streaming problem as an infinite stage discounted Markov decision process (MDP) problem by additionally incorporating past and lower-layer information, allowing a flexible tradeoff between QoE and costs for obtaining system information and solving the problem. In the offline scenario (only with pre-collected data), we propose an enhanced asynchronous advantage actor-critic (eA3C) method by jointly optimizing the parameters of parameterized policy and value function. Specifically, we build an eA3C network consisting of a policy network and a value network that can utilize cross-layer, past, and current information and jointly train the eA3C network using pre-collected samples. In the online scenario (with additional real-time data), we propose two continual learning-based online tuning methods for designing better policies for a specific user with different QoE and training time tradeoffs. In particular, they incorporate different numbers of tunable components into the respective offline trained eA3C networks and adjust the tunable components based on collected real-time samples. Finally, experimental results show that the proposed offline policy can improve the QoE by 6.8% ~ 14.4% compared to the state-of-the-arts in the offline scenario, and the proposed online policies can further achieve 6% ~ 28% gains in QoE over the proposed offline policy in the online scenario.

Index Terms—Adaptive wireless video streaming, lower-layer information, markov decision process (MDP), deep reinforcement learning (DRL), asynchronous advantage actor-critic (A3C), continual learning, online tuning.

I. INTRODUCTION

Video has become the most widely used application on the Internet, witnessing a substantial surge in traffic volume in recent years [2]. Video on demand (VoD) service, which accounts for 29% of the traffic carried over the Internet [2], enables users to, on demand, select and view video content, leveraging the video streaming technology via which

video is delivered and consumed continuously from a source. During video streaming, network fluctuations can easily cause rebuffering at viewers, severely degrading their viewing experiences. To address this issue, adaptive video streaming [8]–[24] has been proposed to adapt the video chunk bitrate to the dynamic network condition and user’s buffer occupancy. In particular, adaptive video streaming can be formulated as a dynamic programming (DP) problem where a (bitrate adaptation) policy that maps the system state to the video chunk bitrate is optimized to maximize the video quality [8]–[24] or to minimize the video quality variation [9]–[16], [18]–[24], rebuffering time [8]–[20], [22]–[24], and startup delay [14], [15].

There are mainly four methods to solve the DP problems for adaptive video streaming [8]–[16]. Firstly, in [8], a heuristic (buffer-based) policy is proposed to select the bitrate of each chunk according to only the instantaneous user’s buffer occupancy without considering the instantaneous network condition. Secondly, [9] presents BOLA that determines the bitrate of each chunk based on the instantaneous user’s buffer occupancy by optimizing the one-step Lyapunov drift (expected change of the Lyapunov function values at two consecutive downloaded video chunks). Both the heuristic [8] and Lyapunov optimization-based [9] policies are myopic and can be far from optimal, as they cannot take into account the instant bitrate adaptation’s long-term (beyond one step) influence. Thirdly, in [10]–[12], the network state evolution is assumed to follow an Markov chain with known transition probabilities, and DP techniques such as value iteration [35, pp. 84] and policy iteration [35, pp. 97] are adopted to solve the DP problems. However, DP may suffer from the curse of modeling as network statistics in practice are usually difficult to obtain. Finally, in [13]–[16], the network statistics are assumed unknown, and reinforcement learning (RL) [33] is applied to resolve the DP problems. The policies obtained by DP and RL can take into account the long-term influence. However, both have high computational complexities due to the curse of dimensionality.

Deep reinforcement learning (DRL) [31]–[33] has been applied to adaptive video streaming to solve the curse of dimensionality issue for RL [17]–[25]. There are two main DRL algorithms, i.e., deep Q-learning (DQ) [17], [18], [27] and asynchronous advantage actor-critic (A3C) [19]–[25]. Specifically, DQ represents Q-factors using a deep Q-network (DQN), adopts a separate copy of the DQN, and trains the DQN with the aid of its copy using deep learning (DL)

L. Zhao and K. Nahrstedt are with University of Illinois Urbana-Champaign, USA. Y. Cui is with IoT Thrust, the Hong Kong University of Science and Technology (Guangzhou), China, and also with The Hong Kong University of Science and Technology, Hong Kong, SAR, China, Y. Jia and Y. Zhang are with Tencent Technology. This paper was submitted in part to IEEE ICC 2024 [1].

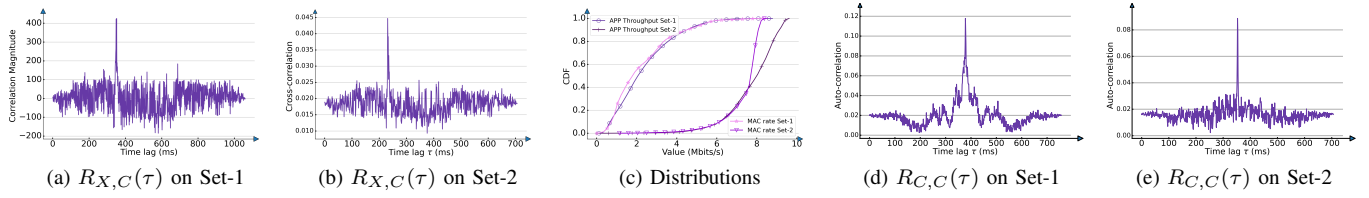


Fig. 1: Relationship between APP layer throughput sequence $\{C_n : n = 1, \dots, N\}$ and MAC rate sequence $\{X_n : n = 1, \dots, N\}$ on two collected datasets [2] (see Section VI for details). The (sample) cross-correlation between X and C and auto-correlation of C are defined as $R_{X,C}(\tau) \triangleq \frac{1}{N-\tau} \sum_{n=1}^{N-\tau} X_n C_{n+\tau}$, $R_{C,C}(\tau) \triangleq \frac{1}{N-\tau} \sum_{n=1}^{N-\tau} C_n C_{n+\tau}$, respectively, where $\tau \in \{0, 1, \dots, N\}$ is time lag, and N is the number of samples.

and Q-learning [27], [34]. The trained DQN produces the approximate Q-factors, and a policy is then obtained by maximizing the approximate Q-factors with respect to all bitrates at each network state. Moreover, A3C represents a randomized policy and a value function using a policy neural network and a value neural network, respectively, and trains these two neural networks alternatively. The trained policy neural network directly produces the optimized randomized policy. A3C naturally balances exploration and exploitation through its randomized policy design and is shown in [19], [20], [24] to achieve better performance than DQ in adaptive video streaming.

Limitations and Motivations: there are three major limitations in the existing work on adaptive video streaming [8]–[24]. Firstly, most of the existing policies [8]–[24] *rely only on application (APP) layer information* (e.g., APP layer throughput, buffer occupancy, and bitrate selection). Since the APP layer relies on all lower layers to complete its process and lower-layers can respond more rapidly to the changes in the environment, information from the lower layers may also be helpful for adaptive video streaming [3], [6]. Fig. 1 (a)–(b) show that the MAC rate can respond 200 – 300 milliseconds faster to the environment changes than the APP layer throughput. This indicates that lower-layer information exposure may help predict the future changes in the application layer and advance its adaptations as suggested in the work item AIS 5G of 3GG [4], [5]. Secondly, A3C [19], [20], [24], [32] breaks the original optimization problem for the policy and value parameters into two separate but related problems and trains the policy and value networks alternatively by solving the optimization problems for the value and policy parameters alternatively. *The training method is rather heuristic* and hardly yields any convergence or performance guarantee. Last but not least, A3C for adaptive video streaming [17]–[20] usually train deep neural networks offline based on the pre-collected samples reflecting a general environment. Offline trained DQ and A3C networks suffer from *potential model mismatches* and yield performance degradation when applied to a particular user since the real-time environment for the specific user, determined by user’s mobility, distance to the transmitter, geographical locations (urban or rural areas), etc., may differ from the general offline environment as shown in Fig. 1.

In this paper, we would like to address the above limitations.

In particular, we boost the performance (users’ QoE) of adaptive wireless video streaming by incorporating lower-layer information in the problem formulation, obtaining an enhanced offline policy via improving the training method for A3C, and fine-tuning the offline policy based on the online collected samples. Our main contributions are summarized below.

- We model the *impacts of lower-layer information* (e.g., downlink media access control (MAC) rate, number of occupied physical resource blocks (PRBs), and modulation and coding scheme (MCS) index) together with the APP layer information on adaptive wireless video streaming. Note that such information is usually not Markovian. By additionally incorporating past and lower-layer information, we formulate a more comprehensive and accurate adaptive wireless video streaming problem as an infinite stage discounted MDP problem, offering possibilities for enhancing QoE. The proposed formulation allows a flexible tradeoff between QoE and costs for obtaining system information and solving the problem.
- We propose an *enhanced A3C method* for the offline scenario (only with pre-collected data), improving the state-of-art A3C method [32]. Specifically, we build an A3C network that consists of a policy neural network and a value neural network to represent a parameterized policy and a parameterized value function, respectively and take cross-layer information and past and current information as input. Moreover, we jointly train the policy and value neural networks (i.e., jointly optimize the policy and value parameters) using pre-collected samples. The joint optimization can capture intrinsic relationship between policy and value parameters and thus achieve fast convergence speed and better convergent performance.
- We propose two *continual learning-based online tuning methods* for the online scenario (with additional real-time data) to design better policies for a specific user leveraging the offline trained A3C network and online collected samples. The first online tuning method builds a new policy network based on the policy network of the offline trained eA3C network, adopts the value network of the offline trained eA3C network, and trains the tunable components of its policy network (i.e., optimizes the newly added parameters of the online policy). The optimization of the tunable components of the new policy network can be viewed as a constrained policy improve-

TABLE I: KEY NOTATION AND ABBREVIATIONS.

Notation	Description
B	buffer size (in seconds)
T	length of each chunk (in seconds)
N (\mathcal{N})	number (set) of chunks
D (\mathcal{D})	number (set) of quality levels
M (\mathcal{M})	number (set) of lower-layer quantities
R_n (\mathcal{R})	bitrate (action) of n -th chunk (bitrate set)
C_n, B_n	APP layer throughput, buffer occupancy at stage n
\mathbf{X}_n	lower-layer quantities at stage n
Y_n	bitrate of $(n-1)$ -th chunk
$S_n \triangleq (B_n, C_n, \mathbf{X}_n, Y_n)$	system state at stage n
$\pi(\cdot; \Theta_\pi)$	parameterized offline policy
$V^\pi(\cdot; \Theta_\pi)$	parameterized value function under offline policy $\pi(\cdot; \Theta_\pi)$
$\hat{\pi}(\cdot; \Theta_{\text{OTP}}, \Theta_\pi^*)$	parameterized online policy of eA3C-OTP
$\hat{V}(\cdot; \Theta_{\text{OTP}}, \Theta_\pi^*)$	parameterized online policy of eA3C-OTPV
$V^{\pi_{\text{OTPV}}}(\cdot; \Theta_\pi^*, \Theta_{\text{OTPV}})$	parameterized value function under online policy $\hat{\pi}(\cdot; \Theta_\pi^*, \Theta_\pi^*)$
Θ_π (Θ_v)	eA3C policy (value) network parameters
Θ_{OTP}	eA3C-OTP policy network tunable parameters
Θ_{OTPV} (Θ_{OTPV}^*)	eA3C-OTPV policy (value) network tunable parameters
Abbreviations	Description
MDP	Markov decision process
APP	Application
PRB	Physical layer resource block
MAC	Media access control
MCS	Modulation and coding scheme
(eA3C) A3C	(Enhanced) asynchronous advantage actor-critic
eA3C-OTP	eA3C with online tuning for policy network
eA3C-OTPV	eA3C with online tuning for policy and value networks
DP	Dynamic programming
DRL	Deep reinforcement learning
DQ	Deep Q-learning
MPC	Model predictive control
RMSP	Root mean squared propagation

ment given the value function under the offline policy. The second online tuning method builds new policy and value networks based on the policy and value networks of the offline trained eA3C network, respectively, and jointly trains the tunable components of its policy and value networks (i.e., jointly optimizes the newly added parameters of the online policy and the value function). The joint optimization of the tunable components of the policy and value networks can be viewed as an online tuning version of the proposed eA3C method. These two continual learning-based online tuning methods produce online policies with better QoE for the specific user than the policy of the offline trained eA3C network. The second online tuning method achieves higher QoE with a longer training time than the first online tuning method.

- We collect a bunch of datasets that contain the APP layer throughput and some lower-layer quantities and evaluate the proposed and existing methods. The experimental results firstly show that the proposed offline policy can improve the QoE by 6.8% \sim 14.4% compared to the state-of-arts in the offline scenario, which reveals the importance of utilizing lower-layer, past and current information and the advantage of the enhanced policy gradient method. The experimental results secondly show that the proposed online policies can achieve 6% \sim 28% gains in QoE compared to the proposed offline policy in the online scenario, indicating the advantage of online tuning for video streaming which is a long-lasting application.

Notation: We represent scalar constants by non-boldface letters (e.g., x), sets by calligraphic letters (e.g., \mathcal{X}), and sets of sets by boldface calligraphic letters (e.g., \mathcal{X}). * denotes the

convolution operation. $\text{vec}(\cdot)$ denotes vectorization. $\mathbf{0}_{M \times M}$ denotes the $M \times M$ zero matrix. \mathbb{N} denotes the set of natural numbers.

II. SYSTEM MODEL

In this section, we introduce the system model for adaptive wireless video streaming using information from the APP layer and lower layers. The key notation and abbreviations used in this paper is listed in Table I.

A. System Model

As illustrated in Fig. 2, we consider adaptive wireless video streaming. On the server side, the video is segmented into N chunks. Let $\mathcal{N} \triangleq \{1, \dots, N\}$ denote the set of video chunks. The length of each chunk is T (in second). The typical value of T is 1 \sim 4. To well adapt to the network conditions, each chunk is pre-encoded into D representations corresponding to D quality levels using High Efficiency Video Coding (HEVC), as in Dynamic Adaptive Streaming over HTTP (DASH). Let $\mathcal{D} \triangleq \{1, \dots, D\}$ denote the set of D quality levels. For ease of exposition, assume that the bitrates of the chunks with the same quality level are identical [8], [10].¹ For all $d \in \mathcal{D}$, the bitrate of the d -th representation of a chunk is denoted by r_d (in bits/s). Note that $r_d, d \in \mathcal{D}$ satisfy $r_1 < \dots < r_D$. Let $\mathcal{R} \triangleq \{r_1, \dots, r_D\}$ denote the set of bitrates corresponding to the D quality levels. The N chunks will be sequentially transmitted to the user (downloaded by the user). For each chunk, only one of the D representations will be transmitted to the user. Let R_n (in bits/s) denote the (APP layer) bitrate of (the representation of) the n -th chunk that is transmitted to the user, where

$$R_n \in \mathcal{R}, n \in \mathcal{N}. \quad (1)$$

Let $C_n \in \mathcal{C}$ represent the average APP layer throughput experienced during the download process for chunk $n \in \mathcal{N}$, where \mathcal{C} denotes the APP layer throughput space which is assumed to be a finite set for simplicity. We model $C_n, n \in \mathcal{N}$ as random variables, since the APP layer throughput usually varies over time (at the scale of seconds) due to the change in large-scale fading (including path loss and shadowing) between the base station and the user caused by the movement of the user, the change in the communication resources allocated to the user, etc.² Then, the download time (in seconds) for chunk n is given by $\frac{R_n T}{C_n}$. As the APP layer relies on all lower-layers to complete its process, and lower-layers are able to respond more rapidly to the changes in the environment as shown in Fig. 1 (a) and (b), information from the lower-layers, such as MAC rate, PRB number, and MCS index, may also be helpful for adaptive wireless video streaming. Therefore, it is important to explicitly model lower-layer information [3], [6], [7]. Specifically, let M and $\mathcal{M} \triangleq \{1, \dots, M\}$ denote the number and set of lower-layer quantities, respectively. For

¹Various chunks of the same quality may have different bitrates due to their distinct spatial redundancies. The variation of bitrates corresponding to the same quality is usually small in practice and hence is ignored for tractability [8], [10].

² C_n reflects the average of small-scale fading over 1 \sim 4 seconds.

all $n \in \mathcal{N}$ and $m \in \mathcal{M}$, let $X_{n,m}$ denote the value of the m -th lower-layer quantity (e.g., MAC rate, PRB number or MCS index) when downloading chunk n , referred to as the m -th lower layer information. Similarly, we model $X_{n,m}, n \in \mathcal{N}, m \in \mathcal{M}$ as random variables to reflect the possible changes over time. Denote $\mathbf{X}_n \triangleq (X_{n,m})_{m \in \mathcal{M}} \in \mathcal{X}$ as the overall lower-layer information when downloading chunk n where \mathcal{X} denotes the overall lower-layer information space which is assumed to be a finite set for simplicity. Mathematically, $C_n, n \in \mathcal{N}$ and $\mathbf{X}_n, n \in \mathcal{N}$ are characterized by probability distributions $\Pr[C_n|C_{n-1}, C_{n-2}, \dots, C_1, \mathbf{X}_n, \mathbf{X}_{n-1}, \dots, \mathbf{X}_1]$ and $\Pr[\mathbf{X}_n|\mathbf{X}_{n-1}, \dots, \mathbf{X}_1]$, respectively.³ It is worth noting that most existing work fails to utilize the lower-layer information in adaptive wireless video streaming, leading to nonnegligible performance loss. The appealing advantages of properly modeling and utilizing lower-layer information will be evidenced in Section VI by extensive experiments.

The N video chunks are downloaded into a playback buffer at the user side, which contains downloaded but as yet unviewed video chunks. Let $B > 0$ denote the buffer size (in seconds) which depends on the policy of the service provider and storage limitation on the user. A typical buffer may hold a few tens of seconds of video chunks. Let $B_n \in [0, B]$ denote the (APP layer) buffer occupancy (in seconds), i.e., the play time of the video chunks left in the buffer, when the user starts to download chunk $n \in \mathcal{N}$. Thus, the buffer occupancy evolves according to⁴

$$B_{n+1} = \left(\left(B_n - \frac{R_n T}{C_n} \right)^+ + T, B \right)^+, \quad n = 1, \dots, N-1, \quad (2)$$

where $(x)^+ \triangleq \max\{x, 0\}$. Let \mathcal{B} denote the buffer occupancy space. Since \mathcal{R} and \mathcal{C} are finite sets, $\frac{R_n}{C_n}$ falls in a finite set, implying that \mathcal{B} is a finite set. Note that $B_n, n \in \mathcal{N}$ are also random due to the randomness of $C_n, n \in \mathcal{N}$. The buffer update equation in (2) indicates that the buffer occupancy increases by T seconds after each chunk is downloaded and decreases as the user watches the video. While downloading chunk n , the buffer occupancy keeps on decreasing if $B_n \geq \frac{R_n T}{C_n}$, as the user is continuously watching the video. The buffer is empty, leading to rebuffering of time $\left(\frac{R_n T}{C_n} - B_n \right)^+$, if $B_n < \frac{R_n T}{C_n}$.

B. Performance Metrics

We refer to the stage where chunk n is being downloaded as stage n , for all $n \in \mathcal{N}$. The system evolves over N stages. We consider three metrics for QoE of video streaming, i.e., video quality, video quality variation, and rebuffering time. Specifically, let $U(R)$ denote the utility for a chunk with the bitrate R . Here, $U(\cdot)$ can be any nonnegative, nondecreasing,

and concave function that is bounded on the finite set \mathcal{D} , and $U(0) = 0$.⁵ Its monotonicity can capture the notion that perceptual quality increases with bitrate. Its concavity can capture the notion that the increase rate of perceptual quality decreases with bitrate. We define the user's QoE at stage n as:

$$g(C_n, B_n, R_n, R_{n-1}) \triangleq U(R_n) - \alpha |U(R_n) - U(R_{n-1})| - \beta \left(\frac{R_n T}{C_n} - B_n \right)^+, \quad (3)$$

where $\alpha > 0$ and $\beta > 0$ are the associated weights for the video quality variation (i.e., quality smoothness) $|U(R_n) - U(R_{n-1})|$ [14], [20] and rebuffering time (i.e., stall time) $\left(\frac{R_n T}{C_n} - B_n \right)^+$ [14], [20], respectively. The weight α and β can be thought of as quantifying the desire to make the video quality variation and rebuffering time small, respectively, and provide the trade-offs among three metrics.

III. QOE MAXIMIZATION PROBLEM FORMULATION

Note that a video usually consists of a large number of chunks (e.g., a 40-minute video contains 600-2400 chunks). Thus, in the rest of the paper, we consider the extreme scenario where $N \rightarrow \infty$, and \mathcal{N} turns to the set of natural numbers, denoted by \mathbb{N} , for tractability. In this section, we formulate the adaptive wireless streaming problem as an infinite stage discounted MDP under certain conditions. Specifically, to ensure a stationary MDP, we first adopt the following assumption.

Assumption 1 (Stationary Markov Chains of Order k): For all $n \in \mathbb{N}$ and for some $k \in \mathbb{N}^+$, the probability distributions $\Pr[C_n|C_{n-1}, C_{n-2}, \dots, C_1, \mathbf{X}_n, \mathbf{X}_{n-1}, \dots, \mathbf{X}_1]$ and $\Pr[\mathbf{X}_n|\mathbf{X}_{n-1}, \dots, \mathbf{X}_1]$ satisfy:

$$\begin{aligned} & \Pr[C_n|C_{n-1}, C_{n-2}, \dots, C_1, \mathbf{X}_n, \mathbf{X}_{n-1}, \dots, \mathbf{X}_1] \\ &= \Pr[C_n|C_{n-1}, C_{n-2}, \dots, C_{n-k}, \mathbf{X}_n, \mathbf{X}_{n-1}, \dots, \mathbf{X}_{n-k}], \\ & \Pr[\mathbf{X}_n|\mathbf{X}_{n-1}, \dots, \mathbf{X}_1] = \Pr[\mathbf{X}_n|\mathbf{X}_{n-1}, \mathbf{X}_{n-2}, \dots, \mathbf{X}_{n-k}], \end{aligned}$$

and are independent of stage n .

Under Assumption 1, $\{(\mathbf{X}_n, \mathbf{X}_{n-1}, \dots, \mathbf{X}_{n-k+1}) : n \in \mathbb{N}\}$ and $\{(C_n, C_{n-1}, \dots, C_{n-k+1}, \mathbf{X}_n, \mathbf{X}_{n-1}, \dots, \mathbf{X}_{n-k+1}) : n \in \mathbb{N}\}$ are stationary Markov chains of order k . Furthermore, we define the system state at stage n , denoted by \mathbf{S}_n , as follows. Given Assumption 1, we include $\mathbf{C}_n \triangleq (C_n, C_{n-1}, \dots, C_{n-k+1})$ and $\bar{\mathbf{X}}_n \triangleq (\mathbf{X}_n, \mathbf{X}_{n-1}, \dots, \mathbf{X}_{n-k+1})$ in \mathbf{S}_n by using state augmentation [34, pp. 38]. Besides, noting that for all $n \in \mathbb{N}$, $g(C_n, B_n, R_n, R_{n-1})$ in (3) depends not only on (C_n, B_n, R_n) but also on R_{n-1} ,⁶ we include R_{n-1} in \mathbf{S}_n by using action augmentation [34, pp. 38]. Specifically, we introduce auxiliary variable Y_n at stage n , and let

$$Y_n = R_{n-1}, \quad n \in \mathbb{N}. \quad (4)$$

Eventually, we have $\mathbf{S}_n \triangleq (B_n, \mathbf{C}_n, \bar{\mathbf{X}}_n, Y_n) \in \mathcal{S}$, where $\mathcal{S} = \mathcal{B} \times \mathcal{C}^k \times \mathcal{X}^k \times \mathcal{R}$ denotes the system state space which is a finite

³We assume that the lower-layer information can be obtained by the user [3], [6], [7].

⁴As in [14], [20], we assume that the user immediately starts to download chunk $n+1$ as soon as chunk n is downloaded. The only exception is that when the buffer is full, the user waits for the buffer to reduce to a certain level, resulting in the suspension of downloading chunk $n+1$.

⁵Logarithmic functions satisfy the requirements on $U(\cdot)$. Besides, numerical results show that Peak Signal-to-Noise Ratio (PSNR) and Structural Similarity Index Measure (SSIM) also satisfy the requirements on $U(\cdot)$ [28], [29].

⁶The video quality and video quality variation are related to R_n and R_{n-1} , the rebuffering time depends on C_n and B_n .

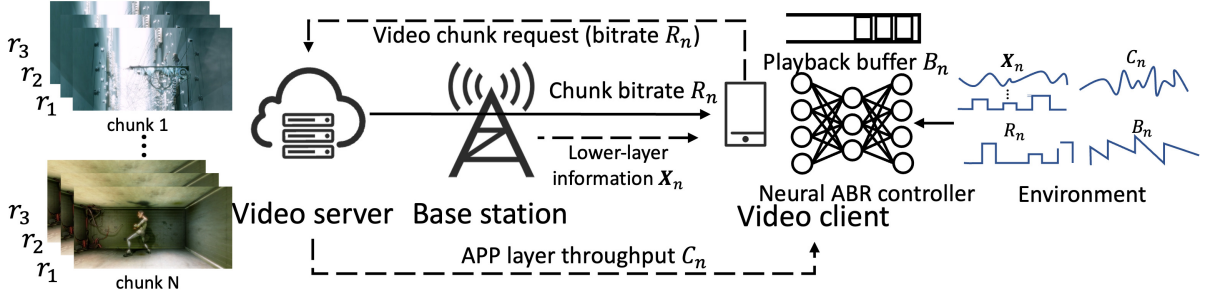


Fig. 2: System model. $D = 3, \mathcal{D} = \{1, 2, 3\}, \mathcal{R} = \{r_1, r_2, r_3\}$.

state space due to the finiteness of \mathcal{B} , \mathcal{C} , \mathcal{X} , and \mathcal{R} . Define $\mathbf{s}_n \triangleq (b_n, \mathbf{c}_n, \bar{\mathbf{x}}_n, y_n), n \in \mathbb{N}$. Therefore, by Assumption 1 and the definition of the system state, we can show the following result on the transition probabilities of the system.

Lemma 1 (Transition Probabilities): For all $n \in \mathbb{N}$,

$$\begin{aligned} & \Pr[\mathbf{S}_{n+1} = \mathbf{s}_{n+1} | \mathbf{S}_n = \mathbf{s}_n, \dots, \mathbf{S}_1 = \mathbf{s}_1, R_n = r_n, \dots, R_1 = r_1] \\ &= \Pr[\mathbf{S}_{n+1} = \mathbf{s}_{n+1} | \mathbf{S}_n = \mathbf{s}_n, R_n = r_n] \\ &= \Pr[\mathbf{C}_{n+1} = \mathbf{c}_{n+1} | \bar{\mathbf{X}}_{n+1} = \bar{\mathbf{x}}_{n+1}, \mathbf{C}_n = \mathbf{c}_n, \bar{\mathbf{X}}_n = \bar{\mathbf{x}}_n] \\ &\times \Pr[\bar{\mathbf{X}}_{n+1} = \bar{\mathbf{x}}_{n+1} | \bar{\mathbf{X}}_n = \bar{\mathbf{x}}_n] \\ &\times \mathbb{I} \left[b_{n+1} = \left(\left(b_n - \frac{r_n T}{c_n} \right)^+ + T, B \right)^+ \right] \times \mathbb{I}[y_{n+1} = r_n], \end{aligned} \quad (5)$$

which is independent of n . Here, $\mathbb{I}[\cdot]$ denotes the indicator function.

Proof 1: Please refer to Appendix A.

Define $\mathbf{s}' = (b', \mathbf{c}', \bar{\mathbf{x}}', y')$ and $\mathbf{s} = (b, \mathbf{c}, \bar{\mathbf{x}}, y)$. Based on Lemma 1, for all $n \in \mathbb{N}$, $\mathbf{s}, \mathbf{s}' \in \mathcal{S}$ and $r \in \mathcal{R}$, we denote $\Pr[\mathbf{S}_{n+1} = \mathbf{s}' | \mathbf{S}_n = \mathbf{s}, R_n = r]$ by $p_{\mathbf{s}, \mathbf{s}'}(r)$, referred to as the transition probability from the system state \mathbf{s} to a successor system state \mathbf{s}' for a given bitrate r .

We refer to the bitrate at stage n , R_n , as the action at stage n and term \mathcal{R} as the action space. Consider a stationary randomized (bitrate adaptation) policy, denoted by π , which is a function that maps the system state \mathbf{s} into a probability distribution $\pi(\mathbf{s}, r), r \in \mathcal{R}$. Note that for all $\mathbf{s} \in \mathcal{S}$, $\pi(\mathbf{s}, \cdot)$ satisfies $\pi(\mathbf{s}, r) \geq 0, r \in \mathcal{R}$ and $\sum_{r \in \mathcal{R}} \pi(\mathbf{s}, r) = 1$. Under Assumption 1 and the stationary randomized policy π , we have a homogeneous Markov chain $\{\mathbf{S}_n : n \in \mathbb{N}\}$ with transition probabilities $\sum_{r \in \mathcal{R}} \pi(\mathbf{s}, r) p_{\mathbf{s}, \mathbf{s}'}(r), \mathbf{s}', \mathbf{s} \in \mathcal{S}$. Given the notion of the system state \mathbf{S}_n , we rewrite $g(\mathbf{C}_n, B_n, R_n, R_{n-1})$ as $g(\mathbf{S}_n, R_n) = U(R_n) - \alpha |U(R_n) - U(Y_n)| - \beta \left(\frac{R_n T}{C_n} - B_n \right)^+$, referred to as the reward at stage n . Thus, given an initial state \mathbf{s} , the value function i.e., expected discounted QoE, under the stationary randomized policy π is given by

$$V^\pi(\mathbf{s}) = \limsup_{N \rightarrow \infty} \mathbb{E} \left[\sum_{n=1}^N \gamma^{n-1} \sum_{r \in \mathcal{R}} \pi(\mathbf{S}_n, r) g(\mathbf{S}_n, r) \right], \quad (6)$$

where $\mathbf{S}_1 = \mathbf{s}$, the system states $\mathbf{S}_n, n = 1, 2, 3, \dots$ evolve according to $\sum_{r \in \mathcal{R}} \pi(\mathbf{s}, r) p_{\mathbf{s}, \mathbf{s}'}(r), \mathbf{s}', \mathbf{s} \in \mathcal{S}$, and the expectation is taken over $\mathbf{S}_n, n = 2, 3, \dots$

We aim to optimize the stationary randomized policy π to maximize the expected discounted QoE given in (6). The problem is readily formulated as follows.

Problem 1 (QoE Maximization):

$$V(\mathbf{s}) = \max_{\pi} \limsup_{N \rightarrow \infty} \mathbb{E} \left[\sum_{n=1}^N \gamma^{n-1} \sum_{r \in \mathcal{R}} \pi(\mathbf{S}_n, r) g(\mathbf{S}_n, r) \right],$$

where $\mathbf{S}_1 = \mathbf{s}$, and $V(\mathbf{s})$ represents the optimal value function. Let π^* denote an optimal stationary randomized policy.

Based on the above illustration, we can conclude that Problem 1 is a stochastic discounted MDP over an infinite number of stages. Note that for all $n \in \mathbb{N}$, $g(\mathbf{S}_n, R_n)$ is bounded since \mathbf{S}_n and R_n lie in finite spaces \mathcal{S} and \mathcal{R} , respectively, and $U(\cdot)$ is bounded on \mathcal{R} . By [35, Proposition 1.2.3] and [35, Proposition 1.2.5], we have the following result.

Lemma 2 (Optimal Value Function and Optimal Stationary Randomized Policy): The optimal value function $V(\cdot)$ satisfies [35, Proposition 1.2.3]:

$$V(\mathbf{s}) = \max_{\pi} V^\pi(\mathbf{s}), \quad \mathbf{s} \in \mathcal{S}, \quad (7)$$

where $V^\pi(\cdot)$ is the value function under the stationary randomized policy π and satisfies:

$$V^\pi(\mathbf{s}) = \sum_{r \in \mathcal{R}} \pi(\mathbf{s}, r) \left(g(\mathbf{s}, r) + \gamma \sum_{\mathbf{s}' \in \mathcal{S}} p_{\mathbf{s}', \mathbf{s}}(r) V^\pi(\mathbf{s}') \right), \quad \mathbf{s} \in \mathcal{S}. \quad (8)$$

Furthermore, an optimal stationary randomized policy π^* is given by [35, Proposition 1.2.5]:

$$\pi^*(\mathbf{s}, r) = \begin{cases} \frac{1}{|\mathcal{R}^*(\mathbf{s})|}, & \text{if } r \in \mathcal{R}^*(\mathbf{s}) \\ 0, & \text{otherwise} \end{cases} \quad \mathbf{s} \in \mathcal{S}, \quad (9)$$

where $\mathcal{R}^*(\mathbf{s}) \triangleq \operatorname{argmax}_{r \in \mathcal{R}} g(\mathbf{s}, r) + \gamma \sum_{\mathbf{s}' \in \mathcal{S}} p_{\mathbf{s}', \mathbf{s}}(r) V(\mathbf{s}')$.

Standard DP algorithms such as value iteration, policy iteration (both applicable for the case where the transition probabilities are known), and Q-learning [35, pp. 495] (applicable for the case where the transition probabilities are unknown) can be used to obtain an optimal stationary policy by solving the Bellman equation given in (7) and (8). However, their computational complexities are prohibitively high due to the extremely large state spaces. Additionally, Assumption 1 may not be satisfied in practical systems, implying that Prob-

lem 1 may not be viewed as a stochastic discounted MDP. Thus, those standard DP may not provide satisfactory QoE in practice. DRL, leveraging DL and approximate DP, is put forward as a solution to address the above limitations. A3C, a widely used DRL algorithm, demonstrates promising potential in the realm of adaptive video streaming. In Section IV and Section V, we present novel methods to enhance the performance of A3C in the offline scenario (only with pre-collected data) and online scenario (with additional real-time data), respectively.

IV. ENHANCED A3C METHOD IN THE OFFLINE SCENARIO

The state-of-art A3C method [32] breaks the original optimization problem for the policy and value parameters into two separate but related problems and alternatively trains the policy and value networks (i.e., solve the optimization problems for the value and policy parameters). Such training method is rather heuristic and hardly yields any convergence or performance guarantee. In this section, we consider the offline scenario only with pre-collected data from many users and present an enhanced A3C (eA3C) method which jointly trains policy and value networks. eA3C captures intrinsic relationship between policy and value parameters and thus reduces training time and improves QoE.

A. Joint Optimization Formulation

We approximate an arbitrary stationary randomized policy π by a parametric form $\pi(\cdot; \Theta_\pi)$, with policy parameters $\Theta_\pi \in \mathbb{R}^{n_\pi}$, and optimize Θ_π instead of π for tractability as in [20], [32]. Specifically, we optimize Θ_π to maximize the expected value function (which is equal to the expected discounted QoE) [32], [33]:

$$\max_{\Theta_\pi} \sum_{\mathbf{s} \in \mathcal{S}} \eta^\pi(\mathbf{s}) V^\pi(\mathbf{s}), \quad (10)$$

where $\eta^\pi(\cdot)$ is the stationary probability distribution of the system state under policy π , and $V^\pi(\cdot)$ is the solution of the Bellman equation in (8) under policy π . Solving the problem in (10) is challenging, since $V^\pi(\cdot)$ is a solution to an extremely large number of equations given by (8) and cannot be obtained analytically. To address the challenge, we equivalently transform the problem in (10) into the problem in (11), as shown at the top of the next page, with $(V^\pi(\mathbf{s}))_{\mathbf{s} \in \mathcal{S}}$ as additional optimization variables, where $\xi > 0$. The equivalence is shown by the following lemma.

Lemma 3 (Relationship between the Problems in (10) and (11)): Consider a sequence $\{\xi^k\}$ with $0 < \xi^k < \xi^{k+1}$ for all $k = 0, 1, 2, \dots$, and $\xi^k \rightarrow \infty$. Then every limit point of the sequence $\{\Theta_\pi^k\}$ is a globally optimal point of the problem in (10), where Θ_π^k represents a globally optimal point of the problem in (11) with $\xi = \xi^k$.

Proof 2: Please refer to Appendix B.

Based on Lemma 3, we can solve the problem in (11) with a sufficiently large ξ for tractability. Note that the problem in (11) is still challenging since the number of optimization variables, $|\mathcal{S}| + n_\pi$, is prohibitively large. As in [20], [32], we approximate the value function under policy π , $V^\pi(\cdot)$, by a

TABLE II: Notation of the weights and layer outputs of the eA3C network ($j = \pi$ or v). For ease of presentation, we let π network and v network represent actor network and critic network, respectively.

Notation	Description
$\mathbf{w}_{i,0}^{(j)} \in \mathbb{R}^{n_{j,0}}$	weight vector of i -th 1D CNN in input layer of j network, $i = 1, \dots, M + 3$
$\mathbf{W}_{j,l} \in \mathbb{R}^{n_{j,l} \times (M+3)(k-n_{j,0}+1)}$	weight matrix of first hidden layer of j network
$\mathbf{W}_{j,l} \in \mathbb{R}^{n_{j,l} \times n_{j,l-1}}$	weight matrix of l -th layers of j network, $l = 2, \dots, L_j - 1$
$\mathbf{w}_{v,L_c} \in \mathbb{R}^{n_{v,L_c}}$	weight vector of output layer of critic network
$\mathbf{W}_{\pi,L_\pi} \in \mathbb{R}^{n_{\pi,L_\pi} \times n_{\pi,L_\pi-1}}$	weight vector of output layer of actor network
$\mathbf{h}_{j,l} \in \mathbb{R}^{n_{j,l}}$	output of l -th layer of j network, $l = 0, 1, \dots, L_j - 1$
$h_{v,L_c} \in \mathbb{R}$	output of L_c -th layer of critic network
$\mathbf{h}_{\pi,L_\pi} \in \mathbb{R}^{n_{\pi,L_\pi}}$	output of L_π -th layer of actor network

parametric form $V^\pi(\cdot; \Theta_v)$, with value parameters $\Theta_v \in \mathbb{R}^{n_v}$. Then, we consider the joint optimization of the policy and value parameters given by the problem in (12), as shown at the top of the next page. Note that it is a simplified version of the problem in (11), and the number of the optimization variables reduces from $|\mathcal{S}| + n_\pi$ to $n_v + n_\pi$. The problem in (12) is generally a non-convex stochastic problem with unknown stationary probability distribution $\eta^\pi(\cdot)$ and transition probabilities $p_{s,s'}(r)$, $\mathbf{s}, \mathbf{s}' \in \mathcal{S}$, $r \in \mathcal{D}$. We can obtain a stationary point of the problem in (12) using standard stochastic gradient methods [40].⁷

B. Neural Network Architecture

We present an actor-critic neural network corresponding to the eA3C method, namely eA3C network. The eA3C network consists of two neural networks, namely actor network (policy network) and critic network (value network), as shown in Figure 3. Specifically, the actor network has weights $\Theta_\pi \in \mathbb{R}^{n_\pi}$ and produces $\pi(\mathbf{s}, r; \Theta_\pi)$, whereas the critic network has weights $\Theta_v \in \mathbb{R}^{n_v}$ and produces $V^\pi(\mathbf{s}; \Theta_v)$. The inputs of the two neural networks are the states over most recent k chunks, \mathbf{S}_n . For ease of implementation, the inputs are rearranged as a $(M + 3) \times k$ matrix, $[\mathbf{C}_n^T \ \mathbf{B}_n^T \ \mathbf{Y}_n^T \ \mathbf{X}_{1,n}^T \ \dots \ \mathbf{X}_{M,n}^T]$. Here, $\mathbf{C}_n \triangleq (C_n, C_{n-1}, \dots, C_{n-k+1}) \in \mathcal{C}^k$ denotes the most recent k APP layer throughputs by stage n ; $\mathbf{B}_n \triangleq (B_n, B_{n-1}, \dots, B_{n-k+1}) \in \mathcal{B}^k$ denotes the most recent k buffer occupancies by stage n ; $\mathbf{Y}_n \triangleq (Y_n, Y_{n-1}, \dots, Y_{n-k+1}) \in \mathcal{D}^k$ denotes the most recent k selected bitrates by stage n ; for all $m = 1, \dots, M$, $\mathbf{X}_{m,n} \triangleq (X_{m,n}, X_{m,n-1}, \dots, X_{m,n-k+1}) \in \mathcal{X}_m^k$ denotes the most recent k m -th lower-layer information by stage n . The notation of the weights and layer outputs of the eA3C network is summarized in Table II.

eA3C actor network: The eA3C actor network has one input layer, $L_\pi - 1$ hidden layers, and one output layer, indexed by $0, 1, \dots, L_\pi - 1, L_\pi$, respectively. The input layer consists of $M + 3$ one-dimensional convolutional neural networks (1D CNNs) which are used to extract the temporal features of the $M + 3$ vectors, $\mathbf{C}_n, \mathbf{B}_n, \mathbf{Y}_n, \mathbf{X}_{1,n}, \dots, \mathbf{X}_{M,n}$, respectively. The lengths of the $M + 3$ 1D CNNs' filters are

⁷One can use standard alternating optimization method to tackle the problem (12). However, it does not guarantee to converge to a stationary point, because the optimization of Θ_π (for fixed Θ_v) and the optimization of Θ_v (for fixed Θ_π) are non-convex and usually cannot be solved optimally [39].

$$\begin{aligned} \max_{\Theta_\pi, (V^\pi(\mathbf{s}))_{\mathbf{s} \in \mathcal{S}}} & \sum_{\mathbf{s} \in \mathcal{S}} \eta^\pi(\mathbf{s}) \sum_{r \in \mathcal{R}} \pi(\mathbf{s}, r; \Theta_\pi) \left(g(\mathbf{s}, r) + \gamma \sum_{\mathbf{s}' \in \mathcal{S}} p_{\mathbf{s}, \mathbf{s}'}(r) V^\pi(\mathbf{s}') \right) \\ & - \xi \sum_{\mathbf{s} \in \mathcal{S}} \eta^\pi(\mathbf{s}) \left(\sum_{r \in \mathcal{R}} \pi(\mathbf{s}, r; \Theta_\pi) \left(g(\mathbf{s}, r) + \gamma \sum_{\mathbf{s}' \in \mathcal{S}} p_{\mathbf{s}, \mathbf{s}'}(r) V^\pi(\mathbf{s}') \right) - V^\pi(\mathbf{s}) \right)^2, \end{aligned} \quad (11)$$

$$\begin{aligned} \max_{\Theta_\pi, \Theta_v} & \sum_{\mathbf{s} \in \mathcal{S}} \eta^\pi(\mathbf{s}) \sum_{r \in \mathcal{R}} \pi(\mathbf{s}, r; \Theta_\pi) \left(g(\mathbf{s}, r) + \gamma \sum_{\mathbf{s}' \in \mathcal{S}} p_{\mathbf{s}, \mathbf{s}'}(r) V^\pi(\mathbf{s}'; \Theta_v) \right) \\ & - \xi \sum_{\mathbf{s} \in \mathcal{S}} \eta^\pi(\mathbf{s}) \left(\sum_{r \in \mathcal{R}} \pi(\mathbf{s}, r; \Theta_\pi) \left(g(\mathbf{s}, r) + \gamma \sum_{\mathbf{s}' \in \mathcal{S}} p_{\mathbf{s}, \mathbf{s}'}(r) V^\pi(\mathbf{s}'; \Theta_v) \right) - V^\pi(\mathbf{s}; \Theta_v) \right)^2. \end{aligned} \quad (12)$$

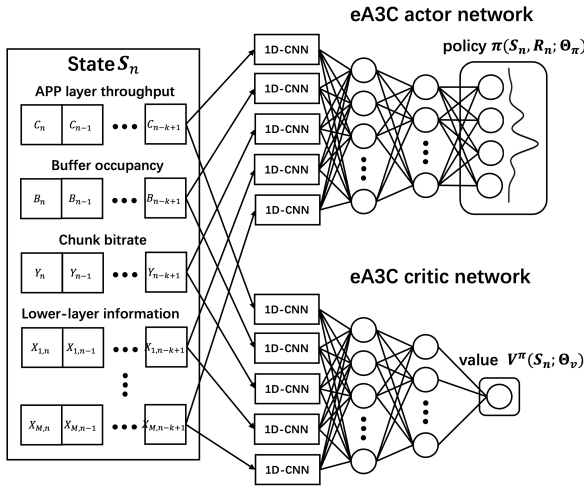


Fig. 3: Structure of the eA3C network

the same, denoted by $n_{\pi,0}$. The l -th hidden layer is a fully connected layer with $n_{\pi,l}$ neurons that utilize the Rectified Linear Unit (ReLU) activation function. The output layer is a fully connected layer with n_{π,L_π} neurons that utilize the softmax activation function. We form a column vector $\Theta_\pi = (\mathbf{w}_{\pi,0}^{(1)}, \mathbf{w}_{\pi,0}^{(2)}, \dots, \mathbf{w}_{\pi,0}^{(M+3)}, \text{vec}(\mathbf{W}_{\pi,1}), \dots, \text{vec}(\mathbf{W}_{\pi,L_\pi})) \in \mathbb{R}^{n_\pi}$, where $n_\pi = (M+3)n_{\pi,0} + n_{\pi,1}(M+3)(k - n_{\pi,0} + 1) + \sum_{l=2}^{L_\pi} n_{\pi,l}n_{\pi,l-1}$, and $\text{vec}(\cdot)$ denotes vectorization. Then, we have:

$$\begin{aligned} \mathbf{h}_{\pi,0} &= (\mathbf{w}_{\pi,0}^{(1)} * \mathbf{C}_n, \mathbf{w}_{\pi,0}^{(2)} * \mathbf{B}_n, \mathbf{w}_{\pi,0}^{(3)} * \mathbf{Y}_n, \mathbf{w}_{\pi,0}^{(4)} * \mathbf{X}_{1,n}, \\ & \quad \mathbf{w}_{\pi,0}^{(5)} * \mathbf{X}_{2,n}, \dots, \mathbf{w}_{\pi,0}^{(M+3)} * \mathbf{X}_{M,n}), \\ \mathbf{h}_{\pi,l} &= \text{ReLU}(\mathbf{W}_{\pi,l} \mathbf{h}_{\pi,l-1}), \quad l = 1, \dots, L_\pi - 1, \\ \mathbf{h}_{\pi,L_\pi} &= \text{Softmax}(\mathbf{W}_{\pi,L_\pi} \mathbf{h}_{\pi,L_\pi-1}), \end{aligned} \quad (13)$$

where $*$ denotes the convolution operation. The output of the network \mathbf{h}_{π,L_π} is the distribution of policy π , i.e., $(\pi(\mathbf{s}, r; \Theta_\pi))_{r \in \mathcal{D}}$.

eA3C critic network: The eA3C critic network has the same neural network structure as the eA3C actor network except that its output layer is a linear neural network without any

activation function. Similarly, the critic network has one input layer, $L_v - 1$ hidden layers, and one output layer, indexed by $0, 1, \dots, L_v - 1, L_v$, respectively. The length of the filter of each 1D CNN and the number of neurons in the l -th layer are $n_{v,0}$ and $n_{v,l}$, respectively. Similarly, we have $\Theta_v = (\mathbf{w}_{v,0}^{(1)}, \mathbf{w}_{v,0}^{(2)}, \dots, \mathbf{w}_{v,0}^{(M+3)}, \text{vec}(\mathbf{W}_{v,1}), \dots, \text{vec}(\mathbf{W}_{v,L_v})) \in \mathbb{R}^{n_v}$, where $n_v = (M+3)n_{v,0} + n_{v,1}(M+3)(k - n_{v,0} + 1) + \sum_{l=2}^{L_v} n_{v,l}n_{v,l-1}$. Then, we have:

$$\begin{aligned} \mathbf{h}_{v,0} &= (\mathbf{w}_{v,0}^{(1)} * \mathbf{C}_n, \mathbf{w}_{v,0}^{(2)} * \mathbf{B}_n, \mathbf{w}_{v,0}^{(3)} * \mathbf{Y}_n, \mathbf{w}_{v,0}^{(4)} * \mathbf{X}_{1,n}, \\ & \quad \mathbf{w}_{v,0}^{(5)} * \mathbf{X}_{2,n}, \dots, \mathbf{w}_{v,0}^{(M+3)} * \mathbf{X}_{M,n}), \\ \mathbf{h}_{v,l} &= \text{ReLU}(\mathbf{W}_{v,l} \mathbf{h}_{v,l-1}), \quad l = 1, \dots, L_v - 1, \\ \mathbf{h}_{v,L_v} &= \mathbf{w}_{v,L_v}^T \mathbf{h}_{v,L_v-1}, \end{aligned} \quad (14)$$

where the output of the network \mathbf{h}_{v,L_v} is the approximated value function under policy π , i.e., $V^\pi(\mathbf{s}; \Theta_v)$.

We consider the offline scenario. Let $\{(\mathbf{C}_n, \mathbf{X}_n) : n = 1, 2, \dots\}$ denote the pre-collected data from a large number of users. Given the sample \mathbf{S}_n at stage n , we generate the action R_n according to the policy distribution $\pi(\mathbf{S}_n, r; \Theta_{\pi,n}), r \in \mathcal{R}$, i.e., $\Pr[R_n = r] = \pi(\mathbf{S}_n, r; \Theta_{\pi,n})$ for all $r \in \mathcal{R}$, and obtain the sample \mathbf{S}_{n+1} at stage $n+1$ as follows: obtain \mathbf{C}_{n+1} and \mathbf{X}_{n+1} from the pre-collected sequence $\{(\mathbf{C}_n, \mathbf{X}_n) : n = 1, 2, \dots\}$; based on \mathbf{C}_n , obtain \mathbf{B}_{n+1} and \mathbf{Y}_{n+1} according to (2) and (4), respectively. Consequently, we have the sample $\mathbf{S}_{n+1} = (\mathbf{C}_{n+1}, \mathbf{X}_{n+1}, \mathbf{B}_{n+1}, \mathbf{Y}_{n+1})$. At each stage n , we use a batch of the latest q samples and choose:

$$\begin{aligned} \sum_{i=n-q}^{n-1} \frac{1}{q} & \left(\log \pi(\mathbf{S}_i, R_i; \Theta_\pi) (g(\mathbf{S}_i, R_i) + \gamma V^\pi(\mathbf{S}_{i+1}; \Theta_v)) \right. \\ & \quad \left. - \xi (g(\mathbf{S}_i, R_i) + \gamma V^\pi(\mathbf{S}_{i+1}; \Theta_v) - V^\pi(\mathbf{S}_i; \Theta_v))^2 \right. \\ & \quad \left. + \beta \sum_{r \in \mathcal{R}} \pi(\mathbf{S}_i, r; \Theta_\pi) \log \pi(\mathbf{S}_i, r; \Theta_\pi) \right) \end{aligned} \quad (15)$$

as the loss function for jointly training the eA3C actor and critic networks. Here, $V^\pi(\cdot; \Theta_v)$ is the output of the critic network, $\sum_{r \in \mathcal{R}} \pi(\mathbf{S}_i, r; \Theta_\pi) \log \pi(\mathbf{S}_i, r; \Theta_\pi)$ is the entropy regularization term, and β is the associated weights for the

entropy. The entropy regularization term is used to ensure adequate exploration of the action space for discovering good policies. Large β encourages policy exploration, whereas small β encourages policy exploitation. We train eA3C network using the root mean squared propagation (RMSP) algorithm [37].

After training, the values of the weights of the actor network and critic network are denoted as $\Theta_\pi^* (\mathbf{w}_{\pi,0}^{*(i)}, i = 1, \dots, M + 3, \mathbf{W}_{\pi,l}^*, l = 1, \dots, L_\pi)$ and $\Theta_v^* (\mathbf{w}_{v,0}^{*(i)}, i = 1, \dots, M + 3, \mathbf{W}_{v,l}^*, l = 1, \dots, L_v - 1, \mathbf{w}_{v,L_v}^*)$, respectively. The output of the actor network $\pi(\mathbf{s}, r; \Theta_\pi^*)$, $r \in \mathcal{R}$ is the resulting policy π . The output of the critic network $V^\pi(\mathbf{s}; \Theta_v^*)$ serves as an approximation of the value function under the policy π .

C. Comparisons with the A3C Method

First, we compare the optimization formulations and solution methods for the policy and value parameters. The proposed joint optimization of policy and value parameters in (12) comes from an equivalent transformation of the problem in (10). By contrast, in [20], [32], the problem in (10) is separated into the two optimization problems for policy parameter Θ_π and value parameter Θ_v , which are given in (16) and (17), respectively, as shown at the top of the next page. The two problems are solved alternatively. The separate optimization method is more heuristic and may yield lower QoE and longer computation time than the joint optimization method as illustrated below. Firstly, applying the standard alternating optimization method [39] to the joint optimization problem in (12) results in two optimization problems that are different from the problems in (16) and (17) and captures more interactions between Θ_π and Θ_v . Note that the objective function of the problem in (16) omits $\sum_{\mathbf{s} \in \mathcal{S}} \eta^\pi(\mathbf{s}) \sum_{r \in \mathcal{R}} \pi(\mathbf{s}, r; \Theta_\pi) (g(\mathbf{s}, r) + \gamma \sum_{\mathbf{s}' \in \mathcal{S}} p_{\mathbf{s}, \mathbf{s}'}(r) V^\pi(\mathbf{s}'; \Theta_v) - V^\pi(\mathbf{s}; \Theta_v))^2$, thereby ignoring some influence of Θ_v . Besides, the objective function of the problem in (17) omits $\sum_{\mathbf{s} \in \mathcal{S}} \eta^\pi(\mathbf{s}) \sum_{r \in \mathcal{R}} \pi(\mathbf{s}, r; \Theta_\pi) (g(\mathbf{s}, r) + \gamma \sum_{\mathbf{s}' \in \mathcal{S}} p_{\mathbf{s}, \mathbf{s}'}(r) V^\pi(\mathbf{s}'; \Theta_v))$, thus ignoring some influence of Θ_π . Secondly, alternatively solving the non-convex problems in (16) and (17) (suboptimally with stationary points) does not have any convergence guarantee to a stationary point of the problem in (12). Next, we compare the network structures and training methods. Firstly, compared to the A3C network in [20], [32], the eA3C network has additional input that is lower-layer information \mathbf{X}_m , $m = 1, \dots, M$. Specifically, one 1D CNN and L fully connected layers are constructed to deal with each lower layer information \mathbf{X}_m . Secondly, unlike [20], [32], we jointly train the actor and critic networks of eA3C network (i.e., jointly optimize the policy and value parameters) which may reduce the training time and improve the QoE. Therefore, it is expected that our proposed eA3C method has higher QoE and shorter training time than the state-of-art A3C method [20], [32], which will be illustrated in Section VI.

V. CONTINUAL LEARNING-BASED ONLINE TUNING METHODS IN THE ONLINE SCENARIO

The offline trained eA3C network based on the pre-collected data from a large number of users has good generalization ability. However, different user may have different wireless network conditions as shown in Fig. 1. The offline trained eA3C network is probably suboptimal for the user due to model mismatches. Since video streaming is a long-lasting application, the real-time samples of a user watching the streaming video can be gradually collected during the video streaming process and used for tailoring the offline policy for this user [24]–[26]. In this section, we consider an online scenario where a specific user is watching a video, starting from stage 0, and its samples, also denoted by $\{(\mathbf{S}_n, R_n) : n = 1, 2, \dots\}$ with a slight abuse of notation, are collected during the video streaming process. We present two continual learning-based online tuning methods to design better policies for the specific user, named online policies, leveraging the eA3C network presented in Section IV and gradually collected real-time samples. We employ a batch of the latest q samples for each round of optimization process of the online tuning methods. At stage $n \in \{1, \dots, q - 1\}$, we use the offline policy obtained from the eA3C network for bitrate adaptation. From stage $n \in \{q, \dots, q' - 1\}$ for some $q' > q$ (collected real-time samples are enough to start the optimization process of online policies, but the optimization process is far from convergent), we still use the offline policy derived from eA3C network for bitrate adaptation but start applying the online tuning methods for designing better online policies. Starting from stage $n \in \{q', \dots\}$, we keep on fine-tuning the online policies while simultaneously using them for bitrate adaptation.

A. Online Tuning for Policy Network

In this part, we present a continual learning-based online tuning method which builds a new policy network based on the eA3C policy network, adopts the eA3C value network, and trains the new component of its policy network using gradually collected real-time samples and the value network. The online tuning method is called the eA3C-OTP method. The resulting network, namely the eA3C-OTP network, consists of an actor network and a critic network and has the same inputs as eA3C network, as shown in Fig. 4 (a). The notation of the weights and layer outputs of the eA3C-OTP network is summarized in Table III.

eA3C-OTP actor network: The eA3C-OTP actor network is built based on the eA3C actor network. It has one input layer, $\hat{L}_\pi - 1$ ($\hat{L}_\pi \geq L_\pi$) hidden layers, and one output layer, indexed by $0, 1, \dots, \hat{L}_\pi - 1, \hat{L}_\pi$, respectively. The input layer has $2(M + 3)$ 1D CNNs, with the first $M + 3$ 1D CNNs coming from the eA3C network. For all $l = 1, \dots, \hat{L}_\pi - 1$, the l -th hidden layer is a partially connected layer containing $n_{\pi,l} + \hat{n}_{\pi,l}$ neurons, with the first $n_{\pi,l}$ neurons coming from the eA3C network and the remaining $\hat{n}_{\pi,l}$ neurons that also utilize the ReLU activation function. For all $l = L_\pi, \dots, \hat{L}_\pi - 1$, the l -th hidden layer is a fully connected layer with $\hat{n}_{\pi,l}$ neurons that utilize the ReLU activation function. The output layer is a fully connected

$$\max_{\Theta_\pi} \sum_{s \in \mathcal{S}} \eta^\pi(s) \sum_{r \in \mathcal{R}} \pi(s, r; \Theta_\pi) \left(g(s, r) + \gamma \sum_{s' \in \mathcal{S}} p_{s, s'}(r) V^\pi(s'; \Theta_v) \right), \quad (16)$$

$$\min_{\Theta_v} \sum_{s \in \mathcal{S}} \eta^\pi(s) \left(\sum_{r \in \mathcal{R}} \pi(s, r; \Theta_\pi) \left(g(s, r) + \gamma \sum_{s' \in \mathcal{S}} p_{s, s'}(r) V^\pi(s'; \Theta_v) \right) - V^\pi(s; \Theta_v) \right)^2. \quad (17)$$

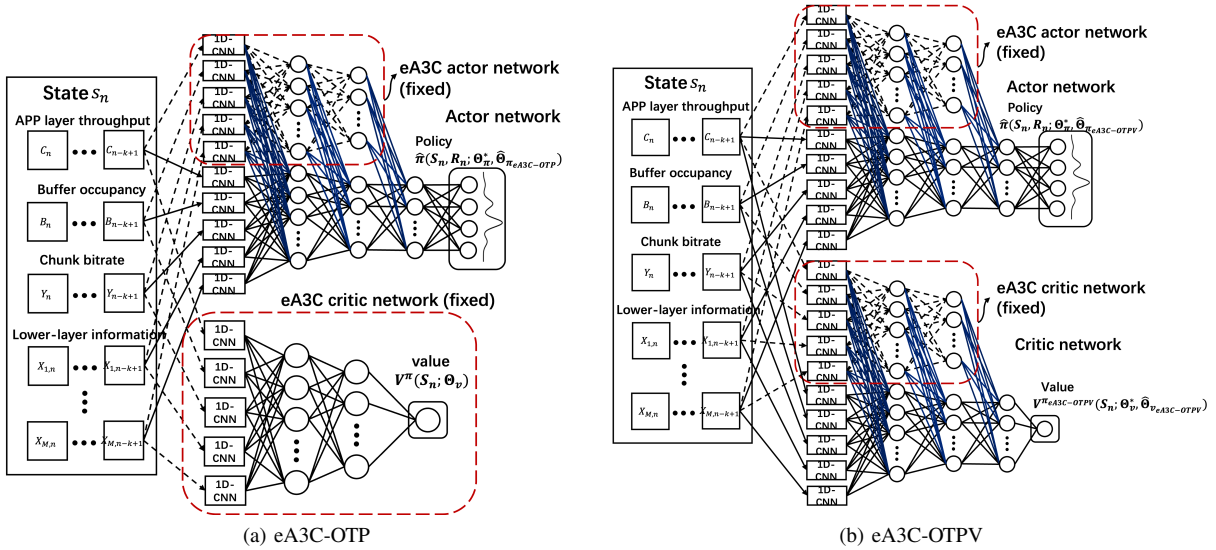


Fig. 4: Structures of the eA3C-OTP and eA3C-OTPV networks.

layer with \hat{n}_π, \hat{L}_π neurons that utilize the softmax activation function. We rearrange all the tunable weights of the eA3C-OTP actor network as a column vector, denoted by $\hat{\Theta}_{\pi_{\text{OTP}}} = (\hat{\mathbf{w}}_{\pi,0}^{(1)}, \hat{\mathbf{w}}_{\pi,0}^{(2)}, \dots, \hat{\mathbf{w}}_{\pi,0}^{(M+3)}, \text{vec}(\hat{\mathbf{W}}_{\pi,1}), \dots, \text{vec}(\hat{\mathbf{W}}_{\pi,\hat{L}_\pi})) \in \mathbb{R}^{\hat{n}_\pi}$, where $\hat{n}_\pi = (M+3)\hat{n}_{\pi,0} + \hat{n}_{\pi,1}(M+3)(2k - \hat{n}_{\pi,0} - n_{\pi,0} + 2) + \sum_{l=2}^{\hat{L}_\pi} \hat{n}_{\pi,l}(\hat{n}_{\pi,l-1} + n_{\pi,l-1}) + \sum_{l=L_\pi+1}^{\hat{L}_\pi} \hat{n}_{\pi,l}\hat{n}_{\pi,l-1}$. Then, based on the structure of the eA3C-OTP actor network, we can derive the layer outputs given by (18), as shown at the top of the next page. Based on the composition structure in (18), the output $\hat{\mathbf{h}}_{\pi,\hat{L}_\pi}$ can be rewritten as $(\hat{\pi}(s, r; \hat{\Theta}_{\pi_{\text{OTP}}}, \Theta_\pi^*))_{r \in \mathcal{D}}$, representing the distribution of a parameterized randomized online policy π_{OTP} . The policy parameters include newly introduced parameters $\hat{\Theta}_{\pi_{\text{OTP}}}$, which will be optimized, and the parameters of the offline policy π , Θ_π^* , which are “frozen” during the online tuning.

eA3C-OTP critic network: We use the trained eA3C critic network as the eA3C-OTP critic network and do not modify its internal structure and weights during the online tuning. In particular, the eA3C-OTP critic network, whose output is $V^\pi(\cdot; \Theta_v^*)$, serves as a facilitator for training the eA3C-OTP actor network.

We aim to optimize the newly added parameters $\hat{\Theta}_{\pi_{\text{OTP}}}$ for the online policy obtained from the eA3C-OTP network to maximize a metric similar to the one defined in (15). Specifically, at each stage $n \geq q$, we use a batch of the latest q samples and choose the loss function given by (19), as shown at the top of the next page, for training the tunable components

of the eA3C-OTP actor network (i.e., optimizing $\hat{\Theta}_{\pi_{\text{OTP}}}$). Since $\pi(\cdot; \Theta_\pi^*)$, whose nested functions are the components of the nested functions of $\hat{\pi}(\cdot; \hat{\Theta}_{\pi_{\text{OTP}}}, \Theta_\pi^*)$, (see (18)), and $V^\pi(\cdot; \Theta_v^*)$ appear in the loss function in (19), the policy and value function obtained from the eA3C network affect the optimal choice of the parameters $\hat{\Theta}_{\pi_{\text{OTP}}}$ for the online policy obtained from the eA3C-OTP network. Intuitively, the optimization of $\hat{\Theta}_{\pi_{\text{OTP}}}$ can be viewed as a constrained⁸ policy improvement given the value function $V^\pi(\cdot; \Theta_v^*)$ under the offline policy π with distribution $\pi(\cdot; \Theta_\pi^*)$. Therefore, it is expected that the eA3C-OTP method has better performance for the specific user than the eA3C method.

We train the eA3C-OTP actor network using the RMSProp algorithm [37]. After training, we denote the values of the tunable weights of the eA3C-OTP actor network by $\hat{\Theta}_{\pi_{\text{OTP}}}^*$. The output of the eA3C-OTP actor network, $\hat{\pi}(s, r; \hat{\Theta}_{\pi_{\text{OTP}}}^*, \Theta_\pi^*)$, is the distribution of the resulting online policy corresponding to eA3C-OTP.

B. Online Tuning for Policy and Value Networks

In this part, we present a continual learning-based online tuning method which builds new policy and value networks based on the policy and value networks of the eA3C network, respectively, and trains the new components of its policy and value networks using gradually collected real-time samples. The online tuning method is called the eA3C-OTPV method.

⁸The online policy subjects to a predetermined parametric form.

TABLE III: Notation of the weights and layer outputs of the eA3C-OTP and eA3C-OTPV networks ($j = \pi$ or v). $\mathbf{w}_{j,0}^{*(i)}$, $i = 1, \dots, M+3$, $\mathbf{W}_{j,l}^*$, $l = 1, \dots, L_j$ are pre-trained weights from the eA3C network and are ‘‘frozen’’ during the online tuning. For ease of presentation, we let π network and v network represent actor network and critic network, respectively. Noting that the policy networks of the eA3C-OTP and eA3C-OTPV networks have the same structure, we do not distinguish the notation for their weights and layer outputs.

eA3C-OTP		eA3C-OTPV	
Notation	Description	Notation	Description
$\mathbf{w}_{j,0}^{*(i)} \in \mathbb{R}^{n_{j,0}}$	weight vector of i -th 1D CNN in input layer of j network, $i = 1, \dots, M+3$	$\mathbf{w}_{j,0}^{*(i)} \in \mathbb{R}^{n_{j,0}}$	weight vector of i -th 1D CNN in input layer of j network, $i = 1, \dots, M+3$
$\hat{\mathbf{w}}_{\pi,0}^{(i)} \in \mathbb{R}^{\hat{n}_{\pi,0}}$	weight vector of i -th 1D CNN in input layer of j network, $i = M+4, \dots, 2(M+3)$	$\hat{\mathbf{w}}_{j,0}^{(i)} \in \mathbb{R}^{\hat{n}_{j,0}}$	weight vector of i -th 1D CNN in input layer of j network, $i = M+4, \dots, 2(M+3)$
$\mathbf{W}_{j,1}^* \in \mathbb{R}^{n_{j,1} \times (M+3)(k-n_{j,0}+1)}$	weight matrix from first $(M+3)$ 1D CNNs in input layer to first $n_{j,1}$ neurons in first hidden layer of j network	$\mathbf{W}_{j,1}^* \in \mathbb{R}^{n_{j,1} \times (M+3)(k-n_{j,0}+1)}$	weight matrix from first $(M+3)$ 1D CNNs in input layer to first $n_{j,1}$ neurons in first hidden layer of j network
$\hat{\mathbf{W}}_{\pi,1} \in \mathbb{R}^{\hat{n}_{\pi,1} \times (M+3)(2k-\hat{n}_{\pi,0}-n_{\pi,0}+2)}$	weight matrix from input layer to remaining $\hat{n}_{\pi,1}$ neurons in first hidden layer of actor network	$\hat{\mathbf{W}}_{j,1} \in \mathbb{R}^{\hat{n}_{j,1} \times (M+3)(2k-\hat{n}_{j,0}-n_{j,0}+2)}$	weight matrix from input layer to remaining $\hat{n}_{j,1}$ neurons in first hidden layer of j network
$\begin{pmatrix} \mathbf{W}_{\pi,1}^* & \mathbf{0}_{n_{\pi,1} \times (k-\hat{n}_{\pi,0}+1)} \\ \hat{\mathbf{W}}_{\pi,1} & \end{pmatrix} \in \mathbb{R}^{(n_{\pi,1}+\hat{n}_{\pi,1}) \times (M+3)(2k-\hat{n}_{\pi,0}-n_{\pi,0}+2)}$	weight matrix from input layer to first hidden layer of actor network	$\begin{pmatrix} \mathbf{W}_{j,1}^* & \mathbf{0}_{n_{j,1} \times (k-\hat{n}_{j,0}+1)} \\ \hat{\mathbf{W}}_{j,1} & \end{pmatrix} \in \mathbb{R}^{(n_{j,1}+\hat{n}_{j,1}) \times (M+3)(2k-\hat{n}_{j,0}-n_{j,0}+2)}$	weight matrix from input layer to first hidden layer of j network
$\mathbf{W}_{j,l}^* \in \mathbb{R}^{n_{j,l} \times n_{j,l-1}}$	weight matrix from first $n_{j,l-1}$ neurons in $(l-1)$ -th layer to first $n_{j,l}$ neurons in l -th layer of j network, $l = 2, \dots, L_j$	$\mathbf{W}_{j,l}^* \in \mathbb{R}^{n_{j,l} \times n_{j,l-1}}$	weight matrix from first $n_{j,l-1}$ neurons in $(l-1)$ -th layer to first $n_{j,l}$ neurons in l -th layer of j network, $l = 2, \dots, L_j$
$\hat{\mathbf{W}}_{\pi,l} \in \mathbb{R}^{\hat{n}_{\pi,l} \times (\hat{n}_{\pi,l-1}+n_{\pi,l-1})}$	weight matrix from $(l-1)$ -th layer to remaining $\hat{n}_{\pi,l}$ neurons in l -th layer of actor network, $l = 2, \dots, L_\pi$	$\hat{\mathbf{W}}_{j,l} \in \mathbb{R}^{\hat{n}_{j,l} \times (\hat{n}_{j,l-1}+n_{j,l-1})}$	weight matrix from $(l-1)$ -th layer to remaining $\hat{n}_{j,l}$ neurons in l -th layer of j network, $l = 2, \dots, L_j$
$\begin{pmatrix} \mathbf{W}_{\pi,l}^* & \mathbf{0}_{n_{\pi,l} \times \hat{n}_{\pi,l-1}} \\ \hat{\mathbf{W}}_{\pi,l} & \end{pmatrix} \in \mathbb{R}^{(n_{\pi,l}+\hat{n}_{\pi,l}) \times (n_{\pi,l-1}+\hat{n}_{\pi,l-1})}$	weight matrix from input layer to first hidden layer of actor network	$\begin{pmatrix} \mathbf{W}_{j,l}^* & \mathbf{0}_{n_{j,l} \times \hat{n}_{j,l-1}} \\ \hat{\mathbf{W}}_{j,l} & \end{pmatrix} \in \mathbb{R}^{(n_{j,l}+\hat{n}_{j,l}) \times (n_{j,l-1}+\hat{n}_{j,l-1})}$	weight matrix from input layer to first hidden layer
$\hat{\mathbf{W}}_{\pi,l} \in \mathbb{R}^{\hat{n}_{\pi,l} \times \hat{n}_{\pi,l-1}}$	weight matrix from $(l-1)$ -th layer to l -th layer of actor network, $l = L_\pi + 1, \dots, \hat{L}_\pi$	$\hat{\mathbf{W}}_{j,l} \in \mathbb{R}^{\hat{n}_{j,l} \times \hat{n}_{j,l-1}}$	weight matrix from $(l-1)$ -th layer to l -th layer of j network, $l = L_j + 1, \dots, \hat{L}_j - 1$
$\hat{\mathbf{h}}_{\pi,0} \in \mathbb{R}^{(M+3)(k-\hat{n}_{\pi,0}+1)}$	output of last $(M+3)$ 1D CNNs in input layer of actor network	$\hat{\mathbf{W}}_{\pi,L_\pi} \in \mathbb{R}^{\hat{n}_{\pi,L_\pi} \times \hat{n}_{\pi,L_\pi-1}}$	weight vector from $(L_\pi - 1)$ -th layer to output layer of actor network
$\hat{\mathbf{h}}_{\pi,t} \in \mathbb{R}^{\hat{n}_{\pi,t}}$	output of last $\hat{n}_{\pi,t}$ neurons in l -th layer of actor network, $l = 1, \dots, L_\pi$	$\hat{\mathbf{w}}_{v,\hat{L}_v} \in \mathbb{R}^{\hat{n}_{v,\hat{L}_v-1}}$	weight vector from $(\hat{L}_v - 1)$ -th layer to output layer of critic network
$\hat{\mathbf{h}}_{\pi,l} \in \mathbb{R}^{\hat{n}_{\pi,l}}$	output of l -th layer of actor network, $l = L_\pi + 1, \dots, \hat{L}_\pi$	$\hat{\mathbf{h}}_{j,0} \in \mathbb{R}^{(M+3)(k-\hat{n}_{j,0}+1)}$	output of last $(M+3)$ 1D CNNs in input layer of j network
		$\hat{\mathbf{h}}_{j,l} \in \mathbb{R}^{\hat{n}_{j,l}}$	output of last $\hat{n}_{j,l}$ neurons in l -th layer of j network, $l = 1, \dots, L_j$
		$\hat{\mathbf{h}}_{j,l} \in \mathbb{R}^{\hat{n}_{j,l}}$	output of l -th layer of j network, $l = L_j + 1, \dots, \hat{L}_j - 1$
		$\hat{h}_{v,\hat{L}_v} \in \mathbb{R}$	output of \hat{L}_v -th layer of critic network
		$\mathbf{h}_{\pi,L_\pi} \in \mathbb{R}^{\hat{n}_{\pi,L_\pi}}$	output of L_π -th layer of actor network

$$\begin{aligned}
\hat{\mathbf{h}}_{\pi,0} &= (\hat{\mathbf{w}}_{\pi,0}^{(1)} * \mathbf{C}_n, \hat{\mathbf{w}}_{\pi,0}^{(2)} * \mathbf{B}_n, \hat{\mathbf{w}}_{\pi,0}^{(3)} * \mathbf{Y}_n, \hat{\mathbf{w}}_{\pi,0}^{(4)} * \mathbf{X}_{1,n}, \dots, \hat{\mathbf{w}}_{\pi,0}^{(M+3)} * \mathbf{X}_{M,n}), \\
(\mathbf{h}_{\pi,1}, \hat{\mathbf{h}}_{\pi,1}) &= \text{ReLU} \left(\begin{pmatrix} \mathbf{W}_{\pi,1}^* & \mathbf{0}_{n_{\pi,1} \times (k-\hat{n}_{\pi,0}+1)} \\ \hat{\mathbf{W}}_{\pi,1} & \end{pmatrix} (\mathbf{h}_{\pi,0}, \hat{\mathbf{h}}_{\pi,0}) \right), \\
(\mathbf{h}_{\pi,l}, \hat{\mathbf{h}}_{\pi,l}) &= \text{ReLU} \left(\begin{pmatrix} \mathbf{W}_{\pi,l}^* & \mathbf{0}_{n_{\pi,l} \times \hat{n}_{\pi,l-1}} \\ \hat{\mathbf{W}}_{\pi,l} & \end{pmatrix} (\mathbf{h}_{\pi,l-1}, \hat{\mathbf{h}}_{\pi,l-1}) \right), \quad l = 2, \dots, L_\pi, \\
\hat{\mathbf{h}}_{\pi,l} &= \text{ReLU}(\hat{\mathbf{W}}_{\pi,l} \hat{\mathbf{h}}_{\pi,l-1}), \quad l = L_\pi + 1, \dots, \hat{L}_\pi - 1, \quad \hat{\mathbf{h}}_{\pi,\hat{L}_\pi} = \text{Softmax}(\hat{\mathbf{W}}_{\pi,L_\pi} \hat{\mathbf{h}}_{\pi,L_\pi-1}).
\end{aligned} \tag{18}$$

$$\begin{aligned}
&\sum_{i=n-q}^{n-1} \frac{1}{q} \left(\log \hat{\pi}(\mathbf{S}_i, R_i; \Theta_\pi^*, \hat{\Theta}_{\pi\text{OTP}}) (g(\mathbf{S}_i, R_i) + \gamma V^\pi(\mathbf{S}_{i+1}; \Theta_v^*)) - \xi (g(\mathbf{S}_i, R_i) + \gamma V^\pi(\mathbf{S}_{i+1}; \Theta_v^*) - V^\pi(\mathbf{S}_i; \Theta_v^*))^2 \right. \\
&\quad \left. + \beta \sum_{r \in \mathcal{R}} \hat{\pi}(\mathbf{S}_i, r; \Theta_\pi^*, \hat{\Theta}_{\pi\text{OTPV}}) \log \hat{\pi}(\mathbf{S}_i, r; \Theta_\pi^*, \hat{\Theta}_{\pi\text{OTPV}}) \right).
\end{aligned} \tag{19}$$

The resulting network, namely the eA3C-OTPV network, consists of an actor network and a critic network and has the same inputs with eA3C, as shown in Fig. 4 (b). The notation of the weights and layer outputs of the eA3C-OTPV network is summarized in Table III.

eA3C-OTPV actor network: The eA3C-OTPV actor network has the same structure as the one of eA3C-OTP. However, different from the eA3C-OTP actor network, the eA3C-OTPV actor network will be jointly trained with the eA3C-OTPV critic network. We omit the details of the network structure due to page limitation and similarly re-

arrange all the tunable weights of the eA3C-OTPV actor network as a column vector, denoted by $\hat{\Theta}_{\pi\text{OTPV}} = (\hat{\mathbf{w}}_{\pi,0}^{(1)}, \hat{\mathbf{w}}_{\pi,0}^{(2)}, \dots, \hat{\mathbf{w}}_{\pi,0}^{(M+3)}, \text{vec}(\hat{\mathbf{W}}_{\pi,1}), \dots, \text{vec}(\hat{\mathbf{W}}_{\pi,\hat{L}_\pi})) \in \mathbb{R}^{\hat{n}_\pi}$, where $\hat{n}_\pi = (M+3)\hat{n}_{\pi,0} + \hat{n}_{\pi,1}(M+3)(2k-\hat{n}_{\pi,0}-n_{\pi,0}+2) + \sum_{l=2}^{L_\pi} \hat{n}_{\pi,l}(\hat{n}_{\pi,l-1}+n_{\pi,l-1}) + \sum_{l=L_\pi+1}^{\hat{L}_\pi} \hat{n}_{\pi,l}\hat{n}_{\pi,l-1}$.

eA3C-OTPV critic network: The eA3C-OTPV critic network is built based on the eA3C critic network. The new neural network has one input layer, $\hat{L}_v - 1$ ($\hat{L}_v \geq L_v$) hidden layers, and one output layer, indexed by $0, 1, \dots, \hat{L}_v - 1, \hat{L}_v$, respectively. The input layer has $2(M+3)$ 1D CNNs, with the first $M+3$ 1D CNNs coming from the eA3C network.

For all $l = 1, \dots, L_v - 1$, the l -th hidden layer is a partially connected layer containing $n_{v,l} + \hat{n}_{v,l}$ neurons, with the first $n_{v,l}$ neurons coming from the eA3C network and the remaining $\hat{n}_{v,l}$ neurons that also utilize the ReLU activation function. For all $l = L_v, \dots, \hat{L}_v - 1$, the l -th hidden layer is a fully connected layer with $\hat{n}_{v,l}$ neurons that utilize the ReLU activation function. The output layer is a fully connected layer without any activation function. Similarly, we rearrange all the tunable weights of the eA3C-OTPV critic network as a column vector, denoted by $\hat{\Theta}_{v\text{OTPV}} = (\hat{\mathbf{w}}_{v,0}^{(1)}, \hat{\mathbf{w}}_{v,0}^{(2)}, \dots, \hat{\mathbf{w}}_{v,0}^{(M+3)}, \text{vec}(\hat{\mathbf{W}}_{v,1}), \dots, \text{vec}(\hat{\mathbf{W}}_{v,\hat{L}_v-1}), \hat{\mathbf{w}}_{v,\hat{L}_v}) \in \mathbb{R}^{\hat{n}_v}$, where $\hat{n}_v = (M+3)\hat{n}_{v,0} + \hat{n}_{v,1}(M+3)(2k - \hat{n}_{v,0} - n_{v,0} + 2) + \sum_{l=2}^{L_v} \hat{n}_{v,l}(\hat{n}_{v,l-1} + n_{v,l-1}) + \sum_{l=L_v+1}^{\hat{L}_v} \hat{n}_{v,l}\hat{n}_{v,l-1}$. Then, based on the structure of the eA3C-OTPV critic network, we can derive the layer outputs given by (20), as shown at the top of the next page. Based on the composition structure in (20), the output \hat{h}_{v,\hat{L}_v} can be rewritten as $V^{\pi\text{OTPV}}(\cdot; \Theta_v^*, \hat{\Theta}_{v\text{OTPV}})$, representing the approximated value function under policy πOTPV . The value parameters include newly introduced parameters $\hat{\Theta}_{v\text{OTPV}}$ which will be optimized and the parameters of the value function from eA3C Θ_v^* which are “frozen” during the online tuning.

We aim to optimize the newly added parameters $\hat{\Theta}_{\pi\text{OTPV}}$ and $\hat{\Theta}_{v\text{OTPV}}$ for the online policy and the value function obtained from the eA3C-OTPV network, respectively, to maximize a metric similar to the one defined in (15). Specifically, at each stage $n \geq q$, we use a batch of the latest q samples and choose the loss function in given by (21), as shown at the top of the next page, for jointly training the tunable components of the actor and critic networks of the eA3C-OTPV network (i.e., optimizing $\hat{\Theta}_{\pi\text{OTPV}}$ and $\hat{\Theta}_{v\text{OTPV}}$). Since $\pi(\cdot; \Theta_\pi^*)$ and $V^\pi(\cdot; \Theta_v^*)$, whose nested functions are components of the nested functions of $\hat{\pi}(\cdot; \Theta_\pi^*, \hat{\Theta}_{\pi\text{OTPV}})$ and $V^{\pi\text{OTPV}}(\cdot; \Theta_v^*, \hat{\Theta}_{v\text{OTPV}})$, respectively, as shown in (18) and (20), appear in the loss function in (21), the policy and value function obtained from the eA3C network affect the optimal choices of the parameters $\hat{\Theta}_{\pi\text{OTPV}}$ and $\hat{\Theta}_{v\text{OTPV}}$ for the online policy and the value function obtained from the eA3C-OTPV network, respectively. Intuitively, the joint optimization of $\hat{\Theta}_{\pi\text{OTPV}}$ and $\hat{\Theta}_{v\text{OTPV}}$ resembles that in the proposed eA3C method in Section IV-A and can be viewed as its online improvement version. Therefore, it is expected that the eA3C-OTPV method has better performance for the specific user than the eA3C method.

Similarly, we train the eA3C-OTPV network using the RMSProp algorithm [37]. After training, we denote the values of the tunable weights of the actor and critic networks of the eA3C-OTPV network by $\hat{\Theta}_{\pi\text{OTPV}}^*$ and $\hat{\Theta}_{v\text{OTPV}}^*$, respectively. The output of the eA3C-OTPV actor network, i.e., $\hat{\pi}(s, r; \hat{\Theta}_{\pi\text{OTPV}}^*, \Theta_\pi^*)$, is the distribution of resulting online policy corresponding to eA3C-OTPV.

C. Comparisons of the eA3C-OTP and eA3C-OTPV Methods

We compare the eA3C-OTP and eA3C-OTPV methods respectively, in terms of QoE, training time, and inference time. Firstly, only the tunable components of the eA3C-OTP policy network are trained based on the policy and value networks of the eA3C network. By contrast, the tunable components of

TABLE IV: Bitrates (in Mbit/s).

Quality level d	1	2	3	4	5	6
Encoding rate r_d (in Mbit/s)	0.3	0.75	1.2	1.85	2.85	4.3

TABLE V: Training setup.

Training Parameter	Offline training	Online training
	Value	
Number of training samples	19200	3200×5
Number of validation samples	6400	—
Number of testing samples	6400	—
Maximization epochs	100	20
Discount factor γ	0.99	0.9
Entropy factor β	Decay from 3 to 0.1	0.5
Learning rate	10^{-4}	10^{-3}
Batch size	8	8
Weight ξ	1	1

both policy and value networks of the eA3C-OTPV network are trained based on the policy and value networks of the eA3C network. Therefore, it is expected that the eA3C-OTPV method outperforms the eA3C-OTP method in QoE. Secondly, the training time for the eA3C-OTPV network is longer than the one for the eA3C-OTP network (and hence q' for the eA3C-OTPV network is larger than the one for the eA3C-OTP network) since it has more tunable parameters and a more complex neural network structure. Thirdly, the inference times for the policies network of the eA3C-OTP and eA3C-OTPV networks to produce the actions (bitrate selections) are identical if their policy networks have the same structure, i.e., the parametric forms $\hat{\pi}(\cdot; \hat{\Theta}_{\pi\text{OTPV}}^*, \Theta_\pi^*)$ and $\hat{\pi}(\cdot; \hat{\Theta}_{\pi\text{OTPV}}^*, \Theta_\pi^*)$ are the same. One can select the eA3C-OTP network or eA3C-OTPV network based on the different QoE, training time, and inference time requirements.

VI. PERFORMANCE EVALUATION

A. Experimental Setup

We consider adaptive streaming of one video, i.e., *En-vividDash3* provided by [38].⁹ The video lasts 192 seconds and is encoded into 48 chunks, each of 4 seconds. That is to say, we set $N = 48$ and $T = 4$ seconds. We set $D = 6$ and set $r_d, d \in \mathcal{D}$ according to Table IV [20]. We set $B = 60$ seconds and adopt the utility function in [20], i.e., $U(R) = \log(\frac{R}{r_1})$. We conduct five experiments under different network environments and collect 5 datasets. Each dataset has multiple traces, each containing 200 samples. Each sample consists of the APP layer throughput and $M = 3$ lower-layer quantities including MAC rate, PRB number, and MCS index. The distributions of the APP layer throughput, MAC rate, PRB number, and MCS index across all datasets are shown in Fig. 5. For all $i = 1, 2, \dots, 5$, we partition the i -th dataset into two subsets with 67% and 33% of samples, named Set- i -OFF and Set- i -ON, respectively. We further divide Set- i -OFF into three subsets with 60%, 20%, and 20% of samples, named Set- i -OFF-Train, Set- i -OFF-Val, and Set- i -OFF-Test, respectively, and merge all samples in Set- i -OFF-Train/Set- i -OFF-Val/Set- i -OFF-Test, $i = 1, 2, \dots, 5$ into

⁹The evaluation results for different videos are similar due to the assumption in footnote 1.

$$\begin{aligned}
\hat{\mathbf{h}}_{v,0} &= (\hat{\mathbf{w}}_{v,0}^{(1)} * \mathbf{C}_n, \hat{\mathbf{w}}_{v,0}^{(2)} * \mathbf{B}_n, \hat{\mathbf{w}}_{v,0}^{(3)} * \mathbf{Y}_n, \hat{\mathbf{w}}_{v,0}^{(4)} * \mathbf{X}_{1,n}, \dots, \hat{\mathbf{w}}_{v,0}^{(M+3)} * \mathbf{X}_{M,n}), \\
(\mathbf{h}_{v,1}, \hat{\mathbf{h}}_{v,1}) &= \text{ReLU} \left(\begin{pmatrix} \mathbf{W}_{v,1}^* & \mathbf{0}_{n_{v,1} \times (k - \hat{n}_{v,0} + 1)} \\ & \hat{\mathbf{W}}_{v,1} \end{pmatrix} (\mathbf{h}_{v,0}, \hat{\mathbf{h}}_{v,0}) \right), \\
(\mathbf{h}_{v,l}, \hat{\mathbf{h}}_{v,l}) &= \text{ReLU} \left(\begin{pmatrix} \mathbf{W}_{v,l}^* & \mathbf{0}_{n_{v,l} \times \hat{n}_{v,l-1}} \\ & \hat{\mathbf{W}}_{v,l} \end{pmatrix} (\mathbf{h}_{v,l-1}, \hat{\mathbf{h}}_{v,l-1}) \right), \quad l = 2, \dots, L_v, \\
\hat{\mathbf{h}}_{v,l} &= \text{ReLU}(\hat{\mathbf{W}}_{v,l} \hat{\mathbf{h}}_{v,l-1}), \quad l = L_v + 1, \dots, \hat{L}_v - 1, \quad \hat{h}_{v,\hat{L}_v} = \hat{\mathbf{w}}_{v,\hat{L}_v}^T \hat{\mathbf{h}}_{v,\hat{L}_v - 1}.
\end{aligned} \tag{20}$$

$$\begin{aligned}
& \sum_{i=n-q}^{n-1} \frac{1}{q} \left(\log \hat{\pi}(\mathbf{S}_i, R_i; \Theta_\pi^*, \hat{\Theta}_{\pi\text{OTPV}}) \left(g(\mathbf{S}_i, R_i) + \gamma V^{\pi\text{OTPV}}(\mathbf{S}_{i+1}; \Theta_v^*, \hat{\Theta}_{v\text{OTPV}}) \right) \right. \\
& \quad \left. - \xi \left(g(\mathbf{S}_i, R_i) + \gamma V^{\pi\text{OTPV}}(\mathbf{S}_{i+1}; \Theta_v^*, \hat{\Theta}_{v\text{OTPV}}) - V^{\pi\text{OTPV}}(\mathbf{S}_i; \Theta_v^*, \hat{\Theta}_{v\text{OTPV}}) \right)^2 \right. \\
& \quad \left. + \beta \sum_{r \in \mathcal{R}} \hat{\pi}(\mathbf{S}_i, r; \Theta_\pi^*, \hat{\Theta}_{\pi\text{OTPV}}) \log \hat{\pi}(\mathbf{S}_i, r; \Theta_\pi^*, \hat{\Theta}_{\pi\text{OTPV}}) \right). \tag{21}
\end{aligned}$$

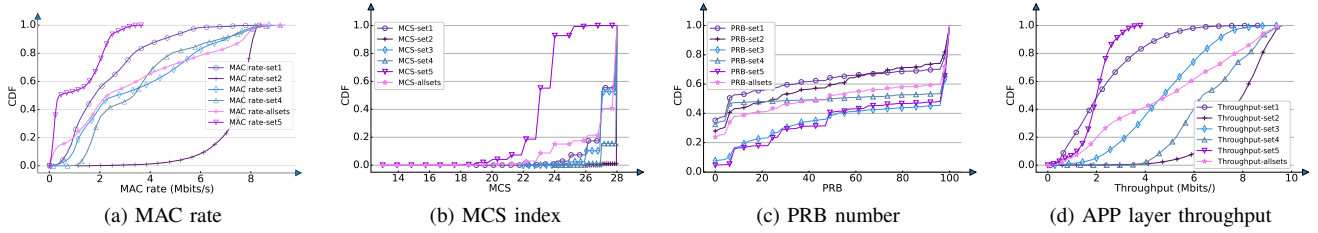


Fig. 5: APP layer throughput and lower-layer information.

one training/validation/testing set, namely Set-OFF-Train/Set-OFF-Val/Set-OFF-Test. The sizes of the datasets are shown in Table V. Set-OFF-Train, Set-OFF-Val, and Set-OFF-Test are used in the offline scenario, whereas Set- i -ON, $i = 1, 2, \dots, 5$ are used in the online scenario. In the rest of the section, we evaluate the proposed eA3C, eA3C-OTP, and eA3C-OTPV methods in terms of the average QoE, inference time, and training time, respectively. We implement eA3C, eA3C-OTP, and eA3C-OTPV on a desktop with the processor of AMD Ryzen 9 5900HX, 16GB RAM, and NVIDIA GeForce RTX 3080 graphics card. Unless otherwise specified, for any DRL-based method, the input of the neural network at stage n includes the APP layer information of the most recent $k = 8$ stages, i.e., APP layer throughputs \mathbf{C}_n , buffer occupancies \mathbf{B}_n , and bitrate selections \mathbf{Y}_n , and for each proposed method, the input of the neural network includes additional lower-layer information (at different amounts) of the most recent $k = 8$ stages. The numbers of neurons and hidden layers of the policy and value networks are set as the same for simplicity, and the average QoE and inference time are for the optimized neural network structure.

B. Offline Scenario

In the offline scenario, we consider five instances of the proposed eA3C method which use different lower-layer in-

formation. Specifically, the instances with one lower-layer quantity ($M = 1$) being MAC rate, PRB number, and MCS index are referred to as eA3C-MAC, eA3C-PRB, eA3C-MCS, respectively; the instance with two lower-layer quantities ($M = 2$) being MCS index and PRB number is referred to as eA3C-2; and the instance with all three lower-layer quantities ($M = 3$) is referred to as eA3C-3. We train the five respective eA3C networks using the proposed eA3C method. We consider three baseline methods, including Pensieve [20], Pensieve-3 (an enhanced version of Pensieve [20] which utilizes all three lower-layer quantities), and MPC [14]. Specifically, Pensieve (Pensieve-3) adopts the A3C method [32] and trains the policy network and value network of the A3C network alternatively. The training setups of all DRL-based methods are identical and are illustrated in Table V. For each DRL-based method, when the value of a loss function on the validation set does not change for five epochs, the training process is stopped, and the corresponding parameters are saved. MPC adapts the video bitrate according to the current APP layer throughput and buffer occupancy based on model predictive control optimization method [35]. Specifically, MPC [14] applies 5-step lookahead optimization [35] and adopts exhaustive search over \mathbb{R}^5 to obtain the optimal bitrate. The details of the proposed and baseline methods are summarized in Table VI. The performance of all methods are evaluated on Set-OFF-Test

TABLE VI: Details of the baseline and proposed methods.

Methods			Input state							Network		Datasets	
			APP layer throughput	buffer occupancy	bitrate selection	MAC rate	PRB	MCS index	M	A3C	eA3C	training	evaluation
Offline scenario	Proposed methods	eA3C-MAC	✓	✓	✓	×	×	×	1	×	✓	Set-OFF-Train	Set-OFF-Test
		eA3C-PRB	✓	✓	✓	×	×	×	1	×	✓		
		eA3C-MCS	✓	✓	✓	×	×	✓	1	×	✓		
		eA3C-2	✓	✓	✓	×	×	✓	2	×	✓		
		eA3C-3	✓	✓	✓	✓	✓	✓	3	×	✓		
	Baseline methods	Pensieve [20]	✓	✓	✓	×	×	×	0	✓	×	Set-OFF-Train	Set-OFF-Test
		Pensieve-3 [32]	✓	✓	✓	×	×	×	3	✓	×	Set-OFF-Train	Set-OFF-Test
		MPC [14]	✓	✓	×	×	×	0	✓	✓	Set-OFF-Train	Set-OFF-Test	
Online scenario	Proposed methods	eA3C-OTP-3	✓	✓	✓	✓	✓	✓	3	×	✓	Set-2(5)-ON	Set-2(5)-ON
		eA3C-OTPV-3	✓	✓	✓	✓	✓	✓	3	×	✓	Set-2(5)-ON	Set-2(5)-ON
		eA3C-3-1set	✓	✓	✓	✓	✓	✓	3	×	✓	Set-2(5)-OFF-Train	Set-2(5)-ON
	Baseline methods	eA3C-3	✓	✓	✓	✓	✓	✓	3	×	✓	Set-OFF-Train	Set-2(5)-ON
		Pensieve [20]	✓	✓	✓	×	×	×	0	✓	×	Set-OFF-Train	Set-2(5)-ON
		MERINA [25]	✓	✓	✓	×	×	×	0	✓	×	Set-OFF-Train	Set-2(5)-ON
		MPC [14]	✓	✓	×	×	×	0	✓	✓	Set-OFF-Train	Set-2(5)-ON	

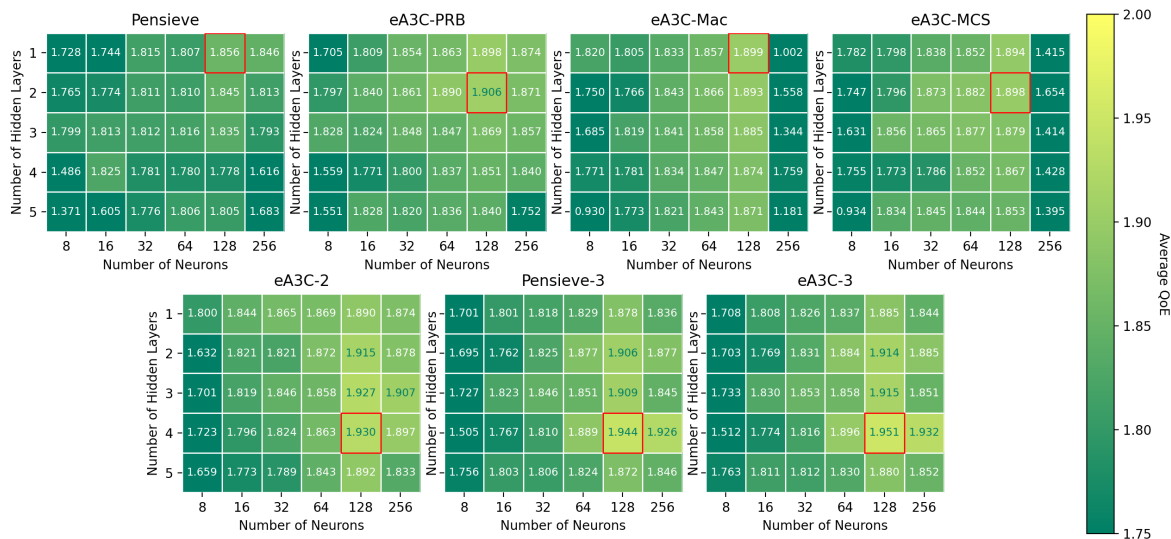


Fig. 6: Heatmaps of the average QoE at $k = 8$ in the offline scenario. The QoE of the optimized neural network structure is marked with a red rectangle.

in the offline scenario.

In the following, we evaluate the proposed eA3C method and the above mentioned baseline methods in the offline scenario. Fig. 6 shows the heatmap of the average QoE at different numbers of neurons and hidden layers. We have the following observations: the average QoE of each method increases and then decreases with the number of neurons; the average QoEs of Pensieve and eA3C-MAC always decrease with the number of hidden layers; and the average QoEs of Pensieve-3, eA3C-MCS, eA3C-PRB, eA3C-2, and eA3C-3 increase and then decrease with the number of hidden layers. These phenomena indicate that overfitting may happen when training a complex neural network, and the structure (numbers of hidden layers and neurons) of the optimized neural network with the maximum QoE is more complex for a larger input size.

Fig. 7 shows all components in the QoE under different weight combinations. From Fig. 7, we can see that the performance of the corresponding QoE component can be improved if more attention (larger weight) is paid (allocated)

to it. This fact indicates that the tradeoff among video quality, video quality variation and rebuffering time can be achieved by choosing different weight combinations.

Fig. 8 shows the average QoE, inference time, and training time versus the number of most recent chunks (k) whose information is input to each network. We can make the following observations. Firstly, the average QoE, inference time, and training time of the proposed eA3C method increase with M , and the average QoE, inference time, and training time of each DRL-based method increase with k . These phenomena imply that the tradeoff among average QoE, inference time, and training time can be achieved by choosing different M and k . Secondly, eA3C-3 outperforms Pensieve-3 in the average QoE and training time and has the same inference time as Pensieve-3. The gains of eA3C-3 over Pensieve-3 in average QoE and training time come from the joint optimization of the policy and value parameters. Their identical inference time derives from the fact that their optimized networks have the same structure. Thirdly, the proposed eA3C method outperforms Pensieve in the average

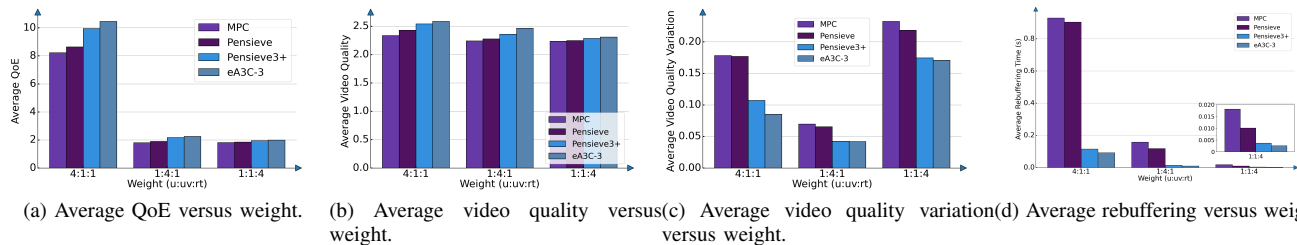


Fig. 7: Individual components in QoE of proposed and baseline schemes under different weights at $k = 8$ in the offline scenario.

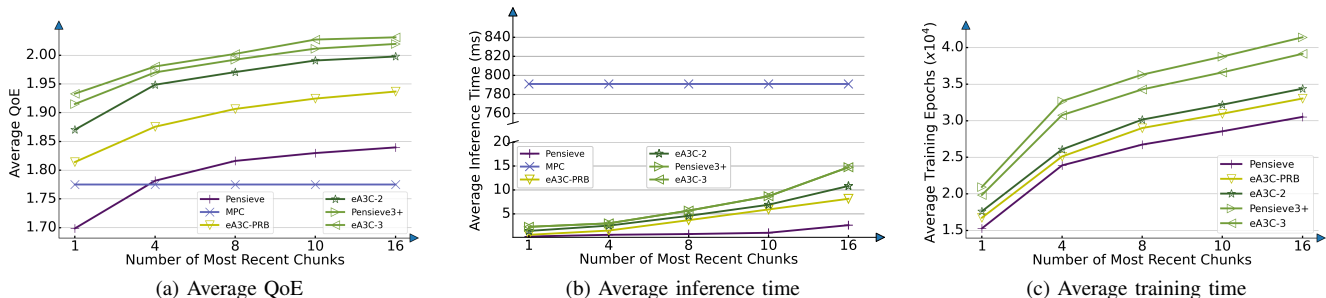


Fig. 8: Different performance metrics of proposed and baseline schemes under different numbers of most recent chunks k in the offline scenario.

QoE at the cost of increased training time and inference time. The gains in QoE of the three instances of the proposed eA3C method over Pensieve (6.8% \sim 13.8%) mainly come from utilizing the lower-layer information (at different amounts). The increased training time and inference time are due to the more complex structures of the optimized eA3C networks for effectively utilizing lower-layer information. Fourthly, the proposed eA3C method outperforms MPC in the average QoE and inference time. The gains of the three instances of the proposed eA3C method over MPC in the average QoE (9.1% \sim 14.4%) come from wise utilization of past and lower-layer information. Their gains over MPC in the average inference time are due to lower computation time for obtaining the bitrate via neural network than exhaustive search. Finally, eA3C-PRB and eA3C-2 at $k = 4$ outperform Pensieve at $k = 16$ in the average QoE, inference time, and training time, implying that a small amount of lower-layer information can compensate for the lack of a large amount of past APP layer information including APP layer throughput, buffer occupancy, and bitrate selection. It becomes evident that judicious utilization of lower-layer information can reduce the memory requirement without compromising performance.¹⁰

C. Online Scenario

In the online scenario, we consider two instances, one for each proposed online tuning method, with all three lower-layer quantities ($M = 3$), namely eA3C-OTP-3 and eA3C-OTPV-3, respectively, to show the maximum achievable QoE

¹⁰eA3C-PRB and eA3C-2 have 16 quantities and 20 quantities as inputs at $k = 4$ while Pensieve has 48 quantities as inputs at $k = 16$.

of the proposed online tuning methods.¹¹ The training setups of the tunable components of the eA3C-OTP-3 and eA3C-OTPV-3 networks are identical and are shown in Table V. The training process lasts over the entire video streaming process. We consider five baseline methods, including eA3C-3, Pensieve [20], eA3C-3-1set, MERINA [25], and MPC [14]. Specifically, eA3C-3 and Pensieve apply the offline trained eA3C and A3C networks in Section VI-B, respectively. eA3C-3-1set uses the same network as eA3C-3 in Section VI-B but trains it in the offline scenario using Set- i -OFF-Train, $i = 2, 5$. MERINA [25] consists of an APP layer throughput prediction network and an A3C network. The prediction network takes the APP layer throughputs of the most recent $k = 8$ stages as input and outputs the predicted future APP layer throughput. The A3C network takes the output of the prediction network as additional input. The two networks are jointly trained in the offline scenario using Set-OFF-Train. eA3C-3-1set and MERINA adopt the same offline training setup as shown in Table V. MPC is the same as the one in Section VI-B. The details of the proposed and baseline methods are summarized in Table VI. The performances of all methods are evaluated on Set- i -ON, $i = 2, 5$.

In the following, we evaluate the two proposed online tuning methods and the above mentioned baseline methods in the online scenario. Fig. 9 shows the heatmaps of the average QoE at different numbers of neurons and hidden layers. We have the following observations: the average QoEs of eA3C-OTP-3 and eA3C-OTPV-3 increase and then decrease with

¹¹It has been shown in Section VI-B that the corresponding offline eA3C method, eA3C-3 achieves the highest QoE.

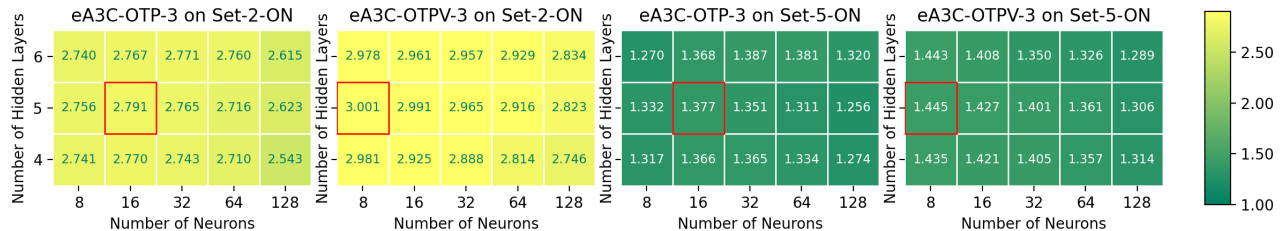


Fig. 9: Heat maps of the average QoE at $k = 8$ in the online scenario. The QoE of the optimized neural network structure is marked with a red rectangle.

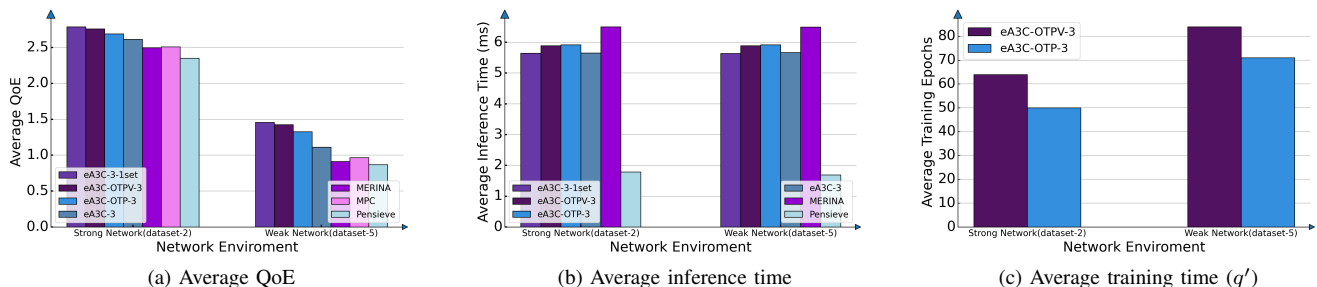


Fig. 10: Different performance metrics of proposed and baseline schemes at $k = 8$ in the online scenario.

the number of hidden layers; the average QoE of eA3C-OTP-3 increases and then decreases with the number of neurons; the average QoE of eA3C-OTPV-3 always decreases with the number of neurons. eA3C-OTPV-3 has a simpler optimized policy network structure than eA3C-OTP-3, as it can also capture input features via the tunable components of its value network.

Fig. 10 shows the average QoE, inference time, and training time under Set-2-ON and Set-5-ON, respectively. Note that Set-2-ON has a larger average APP layer throughput than that of Set-5-ON, as shown in Fig. 5. We can make the following observations from Fig. 10. Firstly, eA3C-3-1set outperforms eA3C-3 in the average QoE (6.6% \sim 31.3%), indicating the model mismatch issue when applying the offline trained eA3C network to the online scenario. Secondly, eA3C-OTP-3 (eA3C-OTPV-3) outperforms eA3C-3 in the average QoE at the cost of increased inference time. Its gain in the average QoE (2.9% \sim 28.3%) arises from online tuning. Its increment in inference time is due to the more complex structure of the policy network. Furthermore, the gain in the average QoE of eA3C-OTP-3 (eA3C-OTPV-3) over eA3C-3 under Set-5-ON (19.4% \sim 28.3%) is higher than that under Set-2-ON (2.9% \sim 5.5%), implying that the gain from online tuning is larger in a weaker network environment. Thirdly, eA3C-OTPV-3 outperforms eA3C-OTP-3 in the average QoE and inference time at the cost of longer training time. Its gain in the average QoE (2.6% \sim 7.4%) comes from adapting the value network to the online environment. Its gain in the average inference time is due to its simpler optimized policy network.

The training time increase arises from training more tunable components (including those in the policy and value networks). Fourthly, eA3C-OTP-3 (eA3C-OTPV-3) exceeds MERINA in the average QoE and inference time. Its gain in the average QoE (7.7% \sim 55.9%) comes from better offline and online designs. Its gain in the average inference time is because MERINA has extra inference time from the prediction network. Finally, eA3C-OTP-3 (eA3C-OTPV-3) outperforms Pensieve at the cost of increased inference time and outperforms MPC in the average QoE and inference time. The gains of eA3C-OTP-3 (eA3C-OTPV-3) over Pensieve and MPC in the average QoE mainly arise from better offline design and online tuning. The increased inference time compared to Pensieve is due to its more complex policy network structure. The reason for the gain over MPC in the average inference time is identical to that illustrated in Section VI-B.

VII. CONCLUSION

This paper focused on enhancing DRL-based adaptive wireless video streaming by incorporating lower-layer information, deriving a rigorous training method, and adopting online tuning with real-time data. We formulated a more comprehensive and accurate infinite stage discounted MDP problem for adaptive wireless video streaming. In the offline scenario (only with pre-collected data), we presented an enhanced A3C method, eA3C, which improves the state-of-art DRL method, A3C, based on lower-layer information and a rigorous training method (based on the joint optimization of the policy and value parameters). In the online scenario (with additional

$$\begin{aligned}
& \Pr[\mathbf{S}_{n+1} = \mathbf{s}_{n+1} | \mathbf{S}_n = \mathbf{s}_n, \dots, \mathbf{S}_1 = \mathbf{s}_1, R_n = r_n, \dots, R_1 = r_1] \\
& \stackrel{(a)}{=} \Pr[\mathbf{C}_{n+1} = \mathbf{c}_{n+1} | \bar{\mathbf{X}}_{n+1} = \bar{\mathbf{x}}_{n+1}, \mathbf{C}_n = \mathbf{c}_n, \bar{\mathbf{X}}_n = \bar{\mathbf{x}}_n] \times \Pr[\bar{\mathbf{X}}_{n+1} = \bar{\mathbf{x}}_{n+1} | \bar{\mathbf{X}}_n = \bar{\mathbf{x}}_n] \\
& \times \Pr[B_{n+1} = b_{n+1}, Y_{n+1} = y_{n+1} | \mathbf{C}_n = \mathbf{c}_n, \dots, \mathbf{C}_1 = \mathbf{c}_1, B_n = b_n, \dots, B_1 = b_1 \\
& \quad , \bar{\mathbf{X}}_n = \bar{\mathbf{x}}_n, \dots, \bar{\mathbf{X}}_1 = \bar{\mathbf{x}}_1, Y_n = y_n, \dots, Y_1 = y_1, R_n = r_n, \dots, R_1 = r_1] \\
& \stackrel{(b)}{=} \Pr[\mathbf{C}_{n+1} = \mathbf{c}_{n+1} | \bar{\mathbf{X}}_{n+1} = \bar{\mathbf{x}}_{n+1}, \mathbf{C}_n = \mathbf{c}_n, \bar{\mathbf{X}}_n = \bar{\mathbf{x}}_n] \times \Pr[\bar{\mathbf{X}}_{n+1} = \bar{\mathbf{x}}_{n+1} | \bar{\mathbf{X}}_n = \bar{\mathbf{x}}_n] \\
& \times \Pr[B_{n+1} = b_{n+1}, Y_{n+1} = y_{n+1} | C_n = c_n, B_n = b_n, Y_n = y_n, R_n = r_n] \\
& \stackrel{(c)}{=} \Pr[\mathbf{C}_{n+1} = \mathbf{c}_{n+1} | \bar{\mathbf{X}}_{n+1} = \bar{\mathbf{x}}_{n+1}, \mathbf{C}_n = \mathbf{c}_n, \bar{\mathbf{X}}_n = \bar{\mathbf{x}}_n] \times \Pr[\bar{\mathbf{X}}_{n+1} = \bar{\mathbf{x}}_{n+1} | \bar{\mathbf{X}}_n = \bar{\mathbf{x}}_n] \\
& \times \mathbb{I} \left[b_{n+1} = \left(\left(b_n - \frac{r_n T}{c_n} \right)^+ + T, B \right)^+ \right] \times \mathbb{I} [y_{n+1} = r_n]. \tag{22}
\end{aligned}$$

real-time data), we presented two continual learning-based online tuning methods, i.e., eA3C-OTP and eA3C-OTPV, for designing better policies for a specific user, which enhance the proposed eA3C method leveraging the offline trained eA3C network and online tuning based on real-time samples. The two online tuning methods compensate each other, providing flexibility to meet diverse QoE and training time requirements. Experimental results show that the proposed eA3C method outperforms the state-of-arts in the offline scenario, and the proposed eA3C-OTP and eA3C-OTPV methods achieve further gains over the proposed eA3C method and surpass the state-of-arts in the online scenario.

APPENDIX A: PROOF OF LEMMA 1

For all $n \in \mathbb{N}$, we can obtain (22), as shown at the top of the current page, where (a) is due to Assumption 1, (b) is due to (2) and (4), and (c) is due to the fact that B_{n+1} is conditionally independent of Y_{n+1} given C_n, B_n, R_n , and Y_{n+1} is conditionally independent of B_{n+1} given R_n . Thus, we can show Lemma 1.

APPENDIX B: PROOF OF LEMMA 3

Firstly, we equivalently convert the problem in (10) to a constrained problem by including $V^\pi(\mathbf{s}), \mathbf{s} \in \mathcal{S}$ and equations in (8) as optimization variables and constraints:

$$\begin{aligned}
& \max_{\Theta_\pi, (V^\pi(\mathbf{s}))_{\mathbf{s} \in \mathcal{S}}} \sum_{\mathbf{s} \in \mathcal{S}} \eta^\pi(\mathbf{s}) V^\pi(\mathbf{s}), \tag{23} \\
& \text{s.t.} \quad (8).
\end{aligned}$$

Next, we transform the constrained problem in (23) into the unconstrained problem in (11) whose objective function is the weighted sum of the objective of the problem in (8) and the penalty for violating the constraints of the problem in (8) by the penalty method [39, pp. 388]. According to [39, Proposition 5.2.1], we can show Lemma 3.

REFERENCES

- [1] L. Zhao, Y. Cui, Y. Jia, Y. Zhang, and K. Nahrstedt, "Enhancing neural adaptive wireless video streaming via lower-layer information exposure," submitted to *Proc. of IEEE ICC*, 2024.
- [2] "Cisco Annual Internet Report (2018–2023) White Paper," 2020. [Online]. Available: <https://www.cisco.com/c/en/us/solutions/collateral/executive-perspectives/annual-internet-report/white-paper-c11-741490.html>
- [3] Y. Xie, and K. Jamieson, "G-scope: Fine-grained telemetry for MextG cellular networks," in *Proc. of ACM Meas. Anal. Comput. Syst.*, vol. 6, no. 1, pp. 1-26, 2022.
- [4] Y. Zhang, G. Li, C. Xiong, Y. Lei, W. Huang, Y. Han, A. Walid, Y.R. Yang, and Z.L. Zhang, "MoWIE: toward systematic, adaptive network information exposure as an enabling technique for cloud-based applications over 5G and beyond," in *Proc. of ACM SIGCOMM NAI*, Aug. 2020, pp. 20-27.
- [5] A.W. Huang, C. Xiong, Y. Lei, Y. Han, and G. Li, "MoWIE for network aware application," *Technical Report*, 2020.
- [6] X. Xie, X. Zhang, S. Kumar, L.E., Li, "piStream: Physical layer informed adaptive video streaming over LTE," in *Proc. of ACM MobiCom*, Sep. 2015, pp. 413-425.
- [7] W. Yuan, K. Nahrstedt, S. V. Adve, D. L. Jones, and R. H. Kravets, "GRACE-1: cross-layer adaptation for multimedia quality and battery energy," *IEEE Trans. Mobile Comput.*, vol. 5, no. 7, pp. 799-815, Jul. 2006.
- [8] T. Huang, R. Johari, N. McKeown, M. Trunnell, and M. Watson, "A buffer-based approach to rate adaptation: Evidence from a large video streaming service," in *Proc. of ACM SIGCOMM*, Aug. 2014, pp. 187-198.
- [9] K. Spiteri, R. Uргаonkar, and R. K. Sitaraman, "BOLA: Near-optimal bitrate adaptation for online videos," *IEEE/ACM Trans. Netw.*, vol. 28, no. 4, pp. 1698-1711, Aug. 2020.
- [10] M. Xing, S. Xiang, and L. Cai, "A real-time adaptive algorithm for video streaming over multiple wireless access networks," *IEEE J. Select. Areas Commun.*, vol. 32, no. 4, pp. 795-805, Apr. 2014.
- [11] C. Zhou, C. Lin, and Z. Guo, "mDASH: A markov decision-based rate adaptation approach for dynamic HTTP streaming," *IEEE Trans. Multimedia*, vol. 18, no. 4, pp. 738-751, Apr. 2016.
- [12] K. Khan and W. Goodridge, "S-MDP: Streaming with markov decision processes," *IEEE Trans. Multimedia*, vol. 21, no. 8, pp. 2012-2025, Aug. 2019.
- [13] M. Claeys, S. Latré, J. Famaey, and F. De Turck, "Design and evaluation of a self-learning HTTP adaptive video streaming client," *IEEE Commun. Lett.*, vol. 18, no. 4, pp. 716-719, Apr. 2014.
- [14] X. Yin, A. Jindal, V. Sekar, and B. Sinopoli, "A control-theoretic approach for dynamic adaptive video streaming over HTTP," in *Proc. of ACM SIGCOMM*, Aug. 2015, pp. 325-338.
- [15] Y. Sun, X. Yin, J. Jiang, V. Sekar, F. Lin, N. Wang, T. Liu, and B. Sinopoli, "CS2P: Improving video bitrate selection and adaptation with data-driven throughput prediction," in *Proc. of ACM SIGCOMM*, Aug. 2016, pp. 272-285.
- [16] F. Y. Yan, H. Ayers, C. Zhu, S. Fouladi, J. Hong, K. Zhang, P.A. Levis, and K. Winstein, 2020, February. "Learning in situ: a randomized experiment in video streaming," in *Proc. of USENIX NSDI*, Feb. 2020, vol. 20, pp. 495-511.
- [17] M. Gadaleta, F. Chiariotti, M. Rossi, and A. Zanella, "D-DASH: A deep Q-learning framework for DASH video streaming," *IEEE Trans. Cogn. Commun. Netw.*, vol. 3, no. 4, pp. 703-718, Dec. 2017.

- [18] R. Bhattacharyya, A. Bura, D. Rengarajan, M. Rumuly, S. Shakkottai, D. Kalathil, R. K. P. Mok, and A. Dhamdhere, "Qflow: A reinforcement learning approach to high qoe video streaming over wireless networks," in *Proc. of ACM MOBIHOC*, Jul. 2019, pp. 251-260.
- [19] S. Sengupta, N. Ganguly, S. Chakraborty, and P. De, "HotDASH: Hotspot aware adaptive video streaming using deep reinforcement learning," in *Proc. of IEEE ICNP*, Sep. 2018, pp. 165-175.
- [20] H. Mao, R. Netravali, and M. Alizadeh, "Neural adaptive video streaming with pensieve," in *Proc. of ACM SIGCOMM*, Aug. 2017, pp. 197-210.
- [21] L. Sun, T. Zong, S. Wang, Y. Liu, and Y. Wang, "Towards optimal low-latency live video streaming," *IEEE/ACM Trans. Netw.*, vol. 29, no. 5, pp. 2327-2338, Oct. 2021.
- [22] L. Cui, D. Su, S. Yang, Z. Wang, and Z. Ming, "TCLiVi: Transmission control in live video streaming based on deep reinforcement learning," *IEEE Trans. Multimedia*, vol. 23, pp. 651-663, Apr. 2021.
- [23] Y. Zhao, Q. Shen, W. Li, T. Xu, W. Niu, and S. Xu, "Latency aware adaptive video streaming using ensemble deep reinforcement learning," in *Proc. of ACM Multimedia*, Oct. 2019, pp. 2647-2651.
- [24] T. Huang et al., "Quality-aware neural adaptive video streaming with lifelong imitation learning," *IEEE J. Select. Areas Commun.*, vol. 38, no. 10, pp. 2324-2342, Oct. 2020.
- [25] N. Kan, Y. Jiang, C. Li, W. Dai, J. Zou, and H. Xiong, "Improving generalization for neural adaptive video streaming via meta reinforcement learning," in *Proc. of ACM Multimedia*, 2022, pp. 3006-3016.
- [26] H. Zhang, A. Zhou, J. Lu, R. Ma, Y. Hu, C. Li, X. Zhang, H. Ma, and X. Chen, "OnRL: improving mobile video telephony via online reinforcement learning," in *Proc. of ACM MobiCom*, Sep. 2020, pp. 1-14.
- [27] H. Van Hasselt, A. Guez, and D. Silver, "Deep reinforcement learning with double q-learning," in *Proc. of AAAI*, vol. 30, no. 1, 2016, Mar.
- [28] G. Correa, P. Assuncao, L. Agostini, and L. A. da Silva Cruz, "Performance and computational complexity assessment of high-efficiency video encoders," *IEEE Trans. Circ. Sys. Video Technol.*, vol. 22, no. 12, pp. 1899-1909, Dec. 2012.
- [29] S. Wang, A. Rehman, Z. Wang, S. Ma, and W. Gao, "Perceptual video coding based on SSIM-inspired divisive normalization," *IEEE Trans. Image Process.*, vol. 22, no. 4, pp. 1418- 1429, Apr. 2013.
- [30] A. A. Rusu, N. C. Rabinowitz, G. Desjardins, H. Soyer, J. Kirkpatrick, K. Kavukcuoglu, R. Pascanu, and R. Hadsell, "Progressive neural networks," *arXiv preprint arXiv:1606.04671*, Sep. 2016.
- [31] D. Silver, A. Huang, C. Maddison, et al. "Mastering the game of Go with deep neural networks and tree search," *Nature*, vol. 529, pp. 484-489, Jan. 2016.
- [32] V. Mnih, A. P. Badia, M. Mirza, A. Graves, T. Lillicrap, T. Harley, D. Silver, and K. Kavukcuoglu, "Asynchronous methods for deep reinforcement learning," in *Proc. of ICML*, Jun. 2016, pp. 1928-1937.
- [33] R. S. Sutton and A. G. Barto, *Reinforcement learning: An introduction*. MIT press, 2018.
- [34] D. Bertsekas, *Dynamic programming and optimal control: Volume I* (Vol. 1). Athena scientific, 2018.
- [35] D. Bertsekas, *Dynamic programming and optimal control: Volume II* (Vol. 2). Athena scientific, 2018.
- [36] M. L. Puterman, *Markov Decision Processes: Discrete Stochastic Dynamic Programming*. Hoboken, NJ, USA: Wiley, 2009.
- [37] G. Hinton, N. Srivastava, and K. Swersky, "Neural networks for machine learning lecture 6a overview of mini-batch gradient descent," 2012, [Online]. Available: <http://www.cs.toronto.edu/~hinton/coursera/lecture6/lec6.pdf>
- [38] "DASH Industry Form. 2016. Reference Client 2.4.0.," 2016. [Online]. Available: <http://mediapm.edgesuite.net/dash/public/nightly/samples/dash-if-reference-player/index.html>
- [39] D. Bertsekas, *Nonlinear programming*. Athena Scientific, 2016.
- [40] L. Bottou, F.E., Curtis, and J. Nocedal, "Optimization methods for large-scale machine learning," *SIAM review*, vol. 60, no. 2, pp.223-311.